

COMMISSIONING OF A 3-D MANUAL MISSING TISSUE COMPENSATOR CUTTER

Nakatudde Rebecca

A research report submitted to the Faculty of Science, University of the Witwatersrand, Johannesburg, in partial fulfilment of the requirements for the degree of Master of Science

Johannesburg, 2008

DECLARATION

I declare that this research report is my own, unaided work. It is being submitted for the degree of Master of Science in the University of the Witwatersrand, Johannesburg. It has not been submitted before for any degree or examination in any other University.

Signed:.....

NAKATUDDE REBECCA

Date:.....

ABSTRACT

Background: Many cancer patients who require external beam radiotherapy such as breast cancer patients, present with irregular surface topographies and tissue inhomogeneities in the treatment field. Such irregularities give rise to unacceptable dose non-uniformity. Standard fields cannot be applied without compensation for missing tissue. 1-D and 2-D missing tissue compensators can be used but they have limitations. 3-D compensators are the most effective but they are normally fabricated using very expensive automated systems.

Objectives: To study the variation of linear attenuation coefficients of different materials in megavoltage photon beams, select a tissue equivalent compensating material and commission a local 3-D manual missing tissue compensator cutter.

Methods and materials: Linear attenuation coefficients were measured for tin, River sand mix, Lincolnshire bolus and dental modelling wax for different energy megavoltage photon beams. Measurements were done in a water phantom using a cylindrical ionisation chamber at varying depths. The CT numbers and densities of the materials were also measured. Negative plaster of paris moulds of the breast and head and neck areas were made using a RANDO™ Alderson anthropomorphic phantom from typically simulated fields. 3-D missing tissue compensators were then fabricated on the manual cutter and were tested for their effectiveness during treatment delivery.

Results: Linear attenuation coefficients were dependent on photon beam energy, the thickness and density of the attenuator, but independent of the depth of measurement for compensator thickness of more than 2 cm. Lincolnshire bolus and dental modelling wax with CT numbers of -78 ± 9 and -88 ± 18 and densities of $1.4 \pm 0.0 \text{ g/cm}^3$ and $0.9 \pm 0.0 \text{ g/cm}^3$ respectively can be regarded as tissue equivalent materials. The fabricated 3-D missing tissue compensators were effective in correcting for dose non-uniformities compared to fields with no beam-modifying devices or wedges (1-D compensators).

Conclusions: The 3-D missing tissue compensators were effective in correcting for dose non-uniformities in treatment fields involving very irregular surface topographies compared to 1-D and 2-D methods. They can be fabricated cheaply using a 3-D manual missing tissue compensator cutter. Quality control procedures need to be followed during fabrication.

Key words: 3-D, manual, missing tissue, compensator and cutter.

DEDICATION

To my husband Neema Godfrey, my mother Kuluda Kibuuka, my children Mbabazi Melissa and Mugisha Maurice, and my brothers and sisters.

To all my friends for their encouragement.

ACKNOWLEDGEMENT

Enormous gratitude to my supervisor, Professor D. G. Van der Merwe, Head of the Division of Medical Physics Charlotte Maxeke Johannesburg Academic Hospital, University of the Witwatersrand Johannesburg. Her dependable and unfailing availability throughout my entire research is acknowledged immensely.

The Johannesburg Radiation Oncology centre is acknowledged for the use of their treatment machines, equipment and materials to conduct this research. Immense indebtedness is due especially to the late Mr. A. Lombaard, Mr. T. B. Moeketsi and Mr. M. Mathoho for designing the equipment used by the author. Mrs. L. Shabangu, Mr. D. Joseph, Mr. A. Rule and Ms. R. Ramashia are particularly thanked for technical guidance.

Professor N. Ssewankambo, Dean Faculty of Medicine, Associate professor E. M. Kiguli, Head Department of Radiology and Dr. J. B. Kigula, Head Department of Radiotherapy all of Makerere University are vastly acknowledged for the encouragement and support during the period of this research.

Qualified gratitude is owed to Schlumberger Foundation and Makerere Faculty Development for the sponsorship during the period in which this work was carried out. All Faculty for the Future women are exceptionally esteemed for their encouragement and keen interest in this work.

Those whose support in one way or another made this work easier than it would otherwise have been include; Engineer. S. Kibuuka, Dr. R. Byanyima, Mr. A. Kavuma, Mr. P. Ddungu, Mr. Y. Shaid and Mr. D. Kagulire. Gratitude is due to them. Greatly appreciated are contributions of others whose mention by names would make an inexhaustive list.

TABLE OF CONTENTS

Declaration.....	ii
Abstract.....	iii
Dedication.....	iv
Acknowledgement.....	v
List of figures.....	viii
List of tables.....	xii
Definition of technical terms and abbreviations.....	xiii

CHAPTER ONE - INTRODUCTION

1.1 Background.....	1
1.2 Historical review of the use of missing tissue compensators.....	4
1.2.1 Description of missing tissue compensators.....	4
1.2.2 Interaction of megavoltage photon beams with tissue.....	5
1.2.3 Types of missing tissue compensators and their limitations.....	7
1.2.3.1 1-D missing tissue compensators.....	7
1.2.3.2 2-D missing tissue compensators.....	7
1.2.3.3 3-D missing tissue compensators.....	7
1.3 Historical review of the methods of fabrication of missing tissue compensators and materials used.....	8
1.3.1 Linear attenuation coefficient.....	11
1.3.2 Effect of linear attenuation coefficient of compensator filling material on the design of missing tissue compensators.....	13
1.4 Statement of the problem.....	14
1.5 Aim of the study.....	15

CHAPTER TWO - METHODS AND MATERIALS

2.1 Determination of linear attenuation coefficient of materials.....	16
2.2 Selection of a tissue equivalent material used in filling hollowed Styrofoam.....	18
2.2.1 CT numbers of the materials.....	18
2.2.2 Densities of the materials.....	19
2.3 Irregular surface contouring and mould formation.....	19
2.3.1 Breast contouring and mould formation.....	19
2.3.2 Head and neck contouring and mould formation.....	25

2.4 Quality control procedures for mould alignment and 3-D missing tissue compensator fabrication at the 3-D manual missing issue compensator cutter.....	28
2.4.1 General approach and quality control of the 3-D manual missing tissue compensator cutter.....	28
2.4.2 Manufacture of breast compensators.....	31
2.4.3 Manufacture of head and neck compensators.....	36
2.5 Film dosimetry to determine the effectiveness of fabricated 3-D missing tissue compensators.....	37
CHAPTER THREE – RESULTS AND DISCUSSION	
3.1 Results of linear attenuation coefficient.....	44
3.2 Results of CT numbers and densities of the materials.....	47
3.3 Results of film dosimetry.....	48
CHAPTER FOUR – RECOMMENDATION AND CONCLUSION	
4.1 Recommendations.....	54
4.2 Conclusion.....	55
5. REFERENCES.....	56
6. APPENDICES.....	59
Appendix A.....	59
Appendix B.....	60
Appendix C.....	62

LIST OF FIGURES

Figure 1- 1: An isodose curve of a beam incident on a patient's irregular surface topography. The dose is normalised to 100% at the isocentre for an equivalent beam perpendicular to a flat surface traversing unit density tissue. The combination of the lower density of the lung and the missing tissue at the surface, result in an isocentric dose of 110% (Gunilla et al., 1989: 205).....	3
Figure 1- 2: Tissue deficit compensation while treating the hatched area at depth with megavoltage photon beam, (a) shows an uncompensated field leading to an uneven dose distribution over the tumour, (b) shows compensation material is in contact with the patient's skin (bolus) and loss of skin sparing is reflected, (c) and (d) show re-establishment of skin sparing and retaining the compensation of bolus by effectively moving the bolus from the patient's surface towards the machine source at the blocking tray position and the compensators are designed out of a tissue equivalent material and high-density material respectively (Stanton and Stinson, 1996).	5
Figure 1- 3: Illustration of the property of skin sparing, (a) shows the dose is proportional to the darkness of the line indicating density of energy absorption, (b) shows the photon (x-ray) intensity is maximum at the surface while maximum dose occurs at d_{max} , the depth of electron equilibrium. (Stanton and Stinson, 1996: 98).	6
Figure 1- 4: A wedge filter is primarily designed to tilt the standard isodose curves through a certain wedge angle (Φ) and the wedge filter isodose curves should be available and used to obtain the composite isodose curves before the filter is used for treatment. The heel transmits less of the initial beam and the toe transmits more.	7
Figure 1- 5: A 2-D compensator constructed out of thin sheets of lead or brass in a stepwise fashion.	9
Figure 1- 6: A Styrofoam cutter fitted with a routing tool used by Boge, R. J to manually construct 2-D compensators.	9
Figure 1- 7: An apparatus used by Khan to construct 3-D compensators in one piece.	10
Figure 1- 8: Scan motion in CT, (a) shows an early design of a CT scanner with the x-ray source and the detector performing a combination of translational and rotational motion, (b) shows a modern CT scanner with the x-ray tube rotating within a stationary circular array of detectors (Khan, 1994).....	12
Figure 1- 9: Schematic representation of thickness h' of a tissue equivalent compensator in relation to the missing tissue thickness h along the same ray (Khan et al., 1970).	13
Figure 1- 10: The 3-D manual missing tissue compensator cutter.....	14
 Figure 2- 1: Experimental set-up for the measurements of the linear attenuation coefficients where, SAD is the Source Axis Distance, SSD is the Source Surface Distance, STD is the Source Tray Distance (56.3 cm and 58.3 cm for linear accelerator and ^{60}Co respectively) and D is the depth of measurement in the water phantom; 3 cm, 5 cm and 6 cm.	17
Figure 2- 2: High-density polystyrene phantom with central hole filled with material.	18
Figure 2- 3: Experimental set-up for the measurements of CT numbers of tin, River sand mix, Lincolnshire bolus, dental modelling wax, water and high-density polystyrene.....	19

Figure 2- 4: Simulation film showing anatomical borders of supraclavicular field of RANDO™ Alderson anthropomorphic phantom's left breast (AL).....	20
Figure 2- 5: Simulation film showing anatomical borders of tangential field of RANDO™ Alderson anthropomorphic phantom's left breast (AL).....	20
Figure 2- 6: Simulation film showing anatomical borders of supraclavicular field of RANDO™ Alderson anthropomorphic phantom's right breast (CR).....	21
Figure 2- 7: Simulation film showing anatomical borders of tangential field of RANDO™ Alderson anthropomorphic phantom's right breast (CR).....	21
Figure 2- 8: Solid wires indicating the references for the right breast tangential field to be used in mould formation. (Similar references were applied to the left breast)..	23
Figure 2- 9: A mould of the left breast made using POP bandages.	24
Figure 2- 10: Mould of the left breast indicating details of the breast type, orientation and reference markings of the field borders.	24
Figure 2- 11: Simulation film showing the anatomical borders of the right lateral field of RANDO™ Alderson anthropomorphic phantom's head and neck.	25
Figure 2- 12: Solid wires indicating the references for the right lateral head and neck field to be used in mould formation. (Similar references were applied to the left lateral field).	26
Figure 2- 13: A mould of the left lateral head and neck made out of POP bandage.	27
Figure 2- 14: A mould of the right lateral head and neck indicating orientation and reference markings of the field borders.....	27
Figure 2- 15: Design of the 3-D manual missing tissue compensator cutter.....	28
Figure 2- 16: Routers of different length.....	29
Figure 2- 17: Demountable portable tape measure used to measure distance IT.	29
Figure 2- 18: Jig systems for mounting the breast and head and neck POP moulds onto the cutter.....	30
Figure 2- 19: Distances and movements used for correct mould mounting and 3-D missing tissue compensator fabrication. (L - Gantry, N- Lateral, M- Vertical, O- Longitudinal, P- Vertical laser and point of interest on the mounted POP mould, Q- Sagittal laser and point of interest on the mounted POP mould).....	30
Figure 2- 20: Movements L, N, M, O, P and Q of the cutter as reflected by similar movements of the treatment machine.....	31
Figure 2- 21: Breast mould mounted on the breast jig system using a straight metal rod.....	32
Figure 2- 22: Alignment of the breast mould at the cutter for the left lateral tangential treatment field during compensator fabrication.	33
Figure 2- 23: Field borders of the treatment area marked onto the Styrofoam.	34
Figure 2- 24: Fabrication of hole into Styrofoam at the cutter.	34
Figure 2- 25: Styrofoam milled according to the contours of the right breast medial tangential field.....	35
Figure 2- 26: Styrofoam filled with Lincolnshire bolus to form 3-D missing tissue compensators for both the lateral and medial tangential fields of the left and right breasts, mounted on the Perspex trays.....	35
Figure 2- 27: Head and neck jig mounted on the flat aluminium plate.....	36
Figure 2- 28: A POP mould of the left lateral head and neck treatment field mounted on the head and neck jig system.....	37
Figure 2- 29: Bisected casts of left breast, right breast and head and neck.....	38
Figure 2- 30: Experimental set-up of the right breast cast at the treatment machine for the right medial tangential field with the gantry such that the back-pointer aligned with the right lateral plane.	40

Figure 2- 31: Film exposed with an open field for the left lateral tangential field of the left breast.....	41
Figure 2- 32: Film exposed with a 30-degree wedge in the treatment field of the left lateral tangential field of the left breast.	41
Figure 2- 33: Film exposed with a manually fabricated 3-D missing tissue compensator in the treatment field of the left lateral tangential.	42
Figure 2- 34: Experimental set-up with 3-D manually fabricated missing tissue compensator in the treatment field of the right lateral tangential with the back pointer aligned to the right medial plane.	42
Figure 2- 35: Film exposed in the open right lateral treatment field of head and neck.	43
Figure 2- 36: Film exposed with 3-D missing tissue compensator in the right lateral treatment field of head and neck.	43
Figure 3- 1: Measured linear attenuation coefficients as a function of the thickness of the tin attenuator measured at different depths in a water phantom.	44
Figure 3- 2: Measured linear attenuation coefficients as a function of the thickness of the River sand mix attenuator measured at different depths in a water phantom.	45
Figure 3- 3: Measured linear attenuation coefficients as a function of the thickness of the Lincolnshire bolus attenuator measured at different depths in a water phantom..	45
Figure 3- 4: Measured linear attenuation coefficients as a function of the thickness of the dental modelling wax attenuator measured at different depths in a water phantom.	46
Figure 3- 5: Verification films of the 3-D compensated right breast medial and lateral tangential treatment fields (the same fields were used for the open and wedged fields).	50
Figure 3- 6: The location of the points used on the six verification films relative to the point O (0,0) for the right breast (right medial and right lateral) tangential fields.	50
Figure 3- 7: The total dose deviation at each point relative to point O (0,0) for the right tangential breast treatment using open fields, wedged fields and 3-D compensated fields. An ideally compensated field would show alignment with the axes, i.e. no variation in dose throughout the field.	50
Figure 3- 8: Verification films of the 3-D compensated left breast medial and lateral tangential treatment fields (the same fields were used for the open and wedged fields).	51
Figure 3- 9: The location of the points used on the six verification films relative to the point O (0,0) for the left breast (left medial and left lateral) tangential fields.....	51
Figure 3- 10: The total dose deviation at each point relative to point O (0,0) for the left tangential breast treatment using open fields, wedged fields and 3-D compensated fields. An ideally compensated field would show alignment with the axes, i.e. no variation in dose throughout the field.....	51
Figure 3- 11: Verification films of the 3-D compensated head and neck treatment fields (the same fields were used for the open and wedged fields).....	52
Figure 3- 12: The location of the points used on the six verification films relative to the point O (0,0) for the head and neck (right lateral and left lateral) treatment fields.	52
Figure 3- 13: The total dose deviation at each point relative to point O (0,0) for the head and neck treatment using open fields, wedged fields and 3-D compensated fields.	52

Figure B 1: Simple interpretation of optical density.....	61
--	----

Figure C 1: Parts used to design The RANDO™ Alderson anthropomorphic phantoms.....	62
--	----

LIST OF TABLES

Table 2- 1: Summary of reference points at simulation for left (AL) and right (CR) breasts	22
Table 2- 2: Summary of reference points at simulation for right and left lateral treatment fields for head and neck.	26
Table 2- 3: Calculated monitor units to deliver the same dose using different beam modifiers in the treatment field.	39
 Table 3- 1: CT numbers of tin, River sand mix, high-density polystyrene, water, Lincolnshire bolus and dental modelling wax measured at three sequential CT mid slices S_1 , S_2 and S_3	47
Table 3- 2: Densities of tin, River sand mix, Lincolnshire bolus and dental modelling wax.	47

DEFINITION OF TECHNICAL TERMS AND ABBREVIATIONS

AL	Left breast size A
CR	Right breast size C
CT	Computed tomography
IAEA	International Atomic Energy Agency
MLC	Multileaf collimator
MV	Megavoltage
PACT	Programme of Action for Cancer Therapy
POP	Plaster of Paris
QART	Quality Assurance in Radiotherapy
QC	Quality Control
TECDOC	Technical Document
TG	Task Group
TRS	Technical Report Series
SAD	Source-axis distance
SSD	Source-surface distance
STD	Source-tray distance
STP	Standard temperature and pressure
1-D	One-dimensional
2-D	Two-dimensional
3-D	Three-dimensional

CHAPTER ONE - INTRODUCTION

1.1 Background

The increased incidence in cancer has resulted in great innovations in its management. Depending on the type of cancer and stage, different modalities including surgery, medical oncology and radiation oncology are used either alone or in combination for cancer management.

Radiation oncology (radiotherapy) is a treatment modality that utilises ionising radiation to treat cancerous cells either from external beams (teletherapy) or internal sources (brachytherapy). Teletherapy involves the use of photons in the kilovoltage range to treat superficial lesions or megavoltage photon and electron beams from linear accelerators or ^{60}Co teletherapy units to treat tumours. The methodology of radiation dose delivery depends on the teletherapy machine, beam energy and treatment technique used. Very few radiotherapy centres in developing countries can afford the full range of radiotherapy equipment (PACT). Often an external beam radiotherapy service is limited to a ^{60}Co teletherapy unit with basic treatment planning and simulation capabilities.

Radiation therapy aims at delivery of the prescribed radiation dose to the target volume as accurately as possible, while minimizing the dose to neighbouring normal tissues and critical structures (Dobbs *et al.*, 1999; Gunilla *et al.*, 1989; Khan, 2003; Podgorsak, 2005; Stanton and Stinson, 1996). Appropriately qualified medical personnel prescribe the radiation dose. However, dose optimisation during treatment delivery can only be achieved with good teamwork from the radiation oncologists, medical physicists and therapy technologists. It is a major role of the licensee to ensure that comprehensive Quality Assurance in Radiotherapy (QART) involving machine installation and calibration, source delivery and safety, operational procedures, clinical dosimetry and the whole treatment planning process is designed and implemented according to national and international recommendations (IAEA-TRS-115, 1994). Quality Control (QC) procedures should be followed before and during treatment. A small error in dose can cause deleterious effects that compromise the already weak patient (Cosset, 2002; Valentin, 2001).

It is frequently in the patient's best interests that radiation treatments are initiated soon after the decision to treat is made. However, it is essential to good radiation therapy that the patient's treatment course be planned and beam-modifying devices be fabricated prior to treatment. Poorly planned and delivered treatment can be more detrimental than no treatment at all (Gunilla *et al.*, 1989). Pre-treatment procedures like patient immobilisation and fabrication of beam-modifying devices should also undergo quality control. The use of beam-modifying devices like missing tissue compensators, beam-shaping blocks and bolus are very useful to individualise and optimise teletherapy fields. This research is aimed at fabricating and testing 3-D missing tissue compensators and in so doing, finalising the design of a manual 3-D missing tissue compensator cutter.

Basic dose distributions and dosimetry measurements on all teletherapy treatment machines are obtained under standard conditions, i.e. homogeneous unit density phantoms using perpendicular beam incidence and flat surfaces. In practice however, the beam may be obliquely incident with respect to the surface, the surface may be curved or irregular in shape and tissue inhomogeneities such as bones and lung may exist in the treatment field as shown in figure 1-1.

Patients with head and neck or breast cancers present with irregular surface topographies and tissue inhomogeneities. Unmodified fields give rise to unacceptable dose distributions within the target volume and excessive irradiation of sensitive structures. Standard dose distributions should not be applied without proper modification or correction (Gunilla *et al.*, 1989; Khan *et al.*, 1970; Khan, 2003; Mira *et al.*, 1982; Papanikolaou *et al.*, 2004; Stanton and Stinson, 1996; Van Dyk *et al.*, 1980).

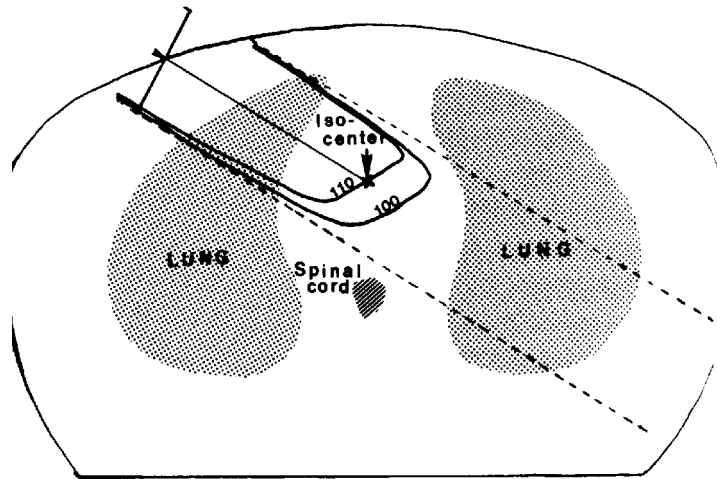


Figure 1- 1: An isodose curve of a beam incident on a patient's irregular surface topography. The dose is normalised to 100% at the isocentre for an equivalent beam perpendicular to a flat surface traversing unit density tissue. The combination of the lower density of the lung and the missing tissue at the surface, result in an isocentric dose of 110% (Gunilla *et al.*, 1989: 205).

Tissue inhomogeneities are volumes within the patient that have non-uniform tissue densities. Whereas most soft tissue have properties that closely approximate that of water, air cavities, metal implants, hard and soft bone are different. Such inhomogeneities encountered in the treatment field, alter the dose distribution from the standard curves due to their attenuation properties. Their effect depends on the incident radiation type and energy.

The effective density of the inhomogeneity is of primary importance in megavoltage photon beams, e.g. bone with a density of 1.8 g/cm^3 attenuates more of the primary photon beam than an equivalent thickness of tissue. This leads to a reduction in the number of photons transmitted by bone and tissues beneath it receive less dose. On the other hand, the presence of air filled cavities allows greater penetration of the primary photon beam than an equivalent thickness of tissue. Thus tissues beneath it receive more dose (Gunilla *et al.*, 1989: 45, 203-205; Stanton and Stinson, 1996: 232).

Several methods have been used to correct for the oblique incidence of radiation beams on body surfaces such as the tissue air ratio method, the effective attenuation correction method and the effective tissue air ratio method (Gunilla *et al.*, 1989).

Monte Carlo algorithms using random sampling methods that require extremely expensive treatment planning systems have also been used. These are expensive and unavailable to most radiation oncology centres in the developing world. The manual isodose shift method of correcting for the same has proved inaccurate in that it uses approximations (Gunilla *et al.*, 1989; Stanton and Stinson, 1996), and has known limitations, e.g. in the angle of incidence (Khan, 2003).

The use of missing tissue compensators in megavoltage photon beams that are shaped to the patient's irregular or curved body surface and of appropriate thickness, is a method of improving dose uniformity in such treatment fields (Ellis and Lescrenier, 1973; Khan, 2003). This report deals with a technique of manual fabrication of 3-D missing tissue compensators for breast and head and neck treatment fields.

1.2 Historical review of the use of missing tissue compensators

1.2.1 Description of missing tissue compensators

Missing tissue compensators are beam-modifying filters fabricated according to the patient's surface contour as part of the pre-treatment procedures (Feaster *et al.*, 1979; Purdy *et al.*, 1977). Their use corrects for non-uniformity in the dose from irregular surface topographies during megavoltage photon beam teletherapy. The skin sparing effect is maintained if the compensator is mounted at a distance of at least 15 cm from the skin of the patient. This distance is considered sufficient to disperse electron and photon scatter (Stanton and Stinson, 1996).

In kilovoltage therapy, tissue equivalent bolus is used as a dose modifier however it is placed on the skin of the patient. The layer of bolus is shaped to the depth of the missing tissue and fits snugly into the irregular surface in order to avoid air pockets that may exist between it and the skin surface (Gunilla *et al.*, 1989). Bolus cannot be used for megavoltage photon beams, as the skin-sparing effect will be lost. Using retracted missing tissue compensators in megavoltage photon beams approximates the use of bolus in kilovoltage therapy as shown in figure 1-2.

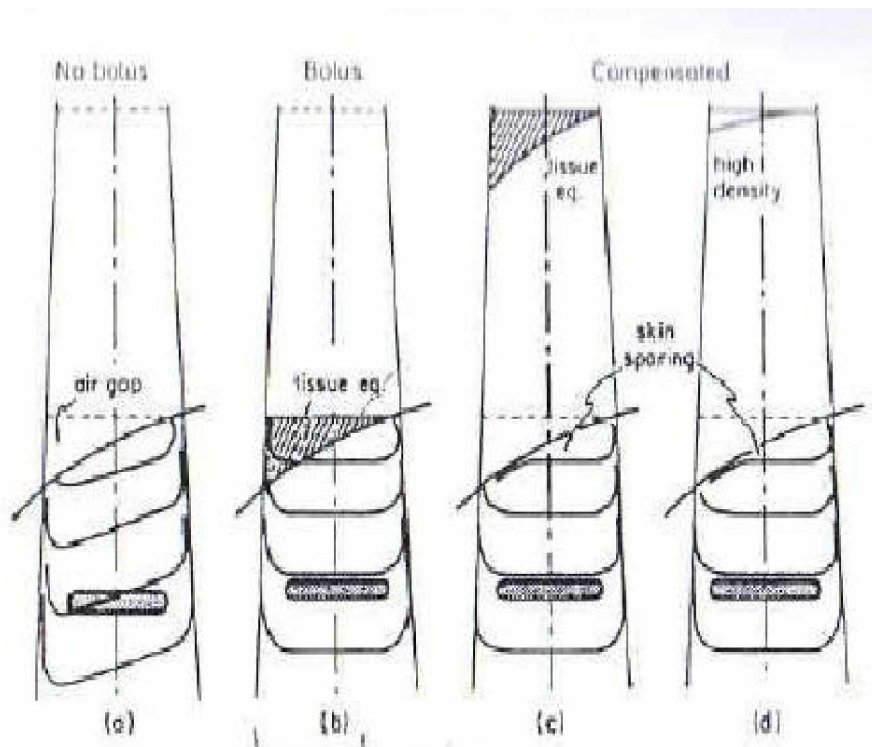


Figure 1- 2: Tissue deficit compensation while treating the hatched area at depth with megavoltage photon beam. Figure (a) shows an uncompensated field leading to an uneven dose distribution over the tumour, (b) shows compensation material is in contact with the patient's skin (bolus) and loss of skin sparing is reflected, (c) and (d) show re-establishment of skin sparing and retaining the compensation of bolus by effectively moving the bolus from the patient's surface towards the machine source at the blocking tray position and the compensators are designed out of a tissue equivalent material and high-density material respectively (Stanton and Stinson, 1996).

1.2.2 Interaction of megavoltage photon beams with tissue

Megavoltage photon beams have an advantage over orthovoltage beams when used to treat deep-seated lesions. They provide greater beam penetration or depth dose due to the lower mass attenuation coefficient in tissue. They also provide a lower skin dose, an effect called skin sparing. The skin sparing effect is due to the way high-energy photons interact with materials. The skin dose decreases because of a characteristic of high-energy photons known as the dose build-up. As megavoltage photon beams enter the patient or the phantom, they set secondary electrons into motion primarily by Compton interactions. This motion is predominantly in the forward direction, thus a net flow of electrons is produced with depth in the patient. The concurrent slowing of these electrons is accompanied with deposition of energy and a rise in dose with depth

in the patient. The superficial tissue therefore receives less dose as compared to the depth of maximum dose as shown in figure 1-3.

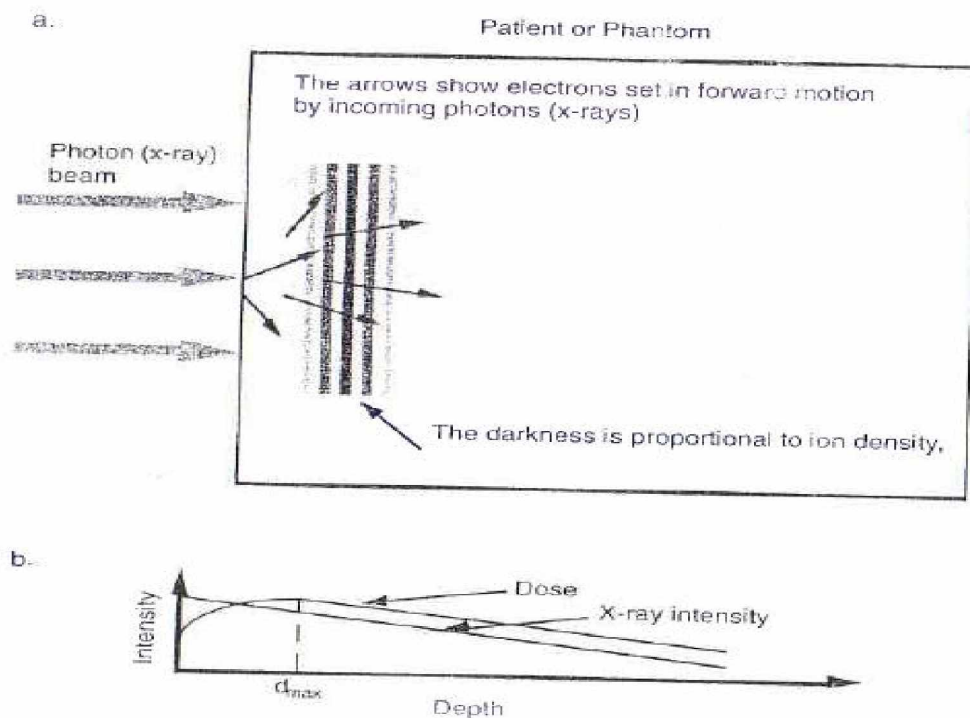


Figure 1- 3: Illustration of the property of skin sparing, (a) shows the dose is proportional to the darkness of the line indicating density of energy absorption, (b) shows the photon (x-ray) intensity is maximum at the surface while maximum dose occurs at d_{max} , the depth of electron equilibrium. (Stanton and Stinson, 1996: 98).

In photon therapy, the maximum dose (D_{max}) occurs at the point at which the energy of the electrons coming to rest equals to the energy of electrons being set into motion by new photon interactions. Electron equilibrium is the point at which equal numbers of electrons are being stopped and driven forward or where kerma equals dose. The depth at which this occurs is called the d_{max} . The depth of electron equilibrium (d_{max}) increases with energy because the range of the electrons set into motion by the photons increases with increasing photon energy (Stanton and Stinson, 1996: 100).

A retracted missing tissue compensator also results theoretically in some under dose at depth compared to bolus. This occurs because once the missing tissue volume is placed at some distance away from the patient, it removes the scatter from that

volume that would otherwise have contributed to the dose to the underlying tissue (Khan *et al.*, 1970).

1.2.3 Types of missing tissue compensators and their limitations

1.2.3.1 1-D missing tissue compensators

Wedge filters are examples of 1-D compensators. They are non-customised devices and are fabricated from metals such as copper, steel, brass or lead. However, their use as compensators is limited to oblique beam incidence of surfaces in which the contour can be approximated to a plane that is at an angle Φ to the beam. Compensation is then achieved in one-dimension by using a wedge of angle Φ as shown in figure 1-4.

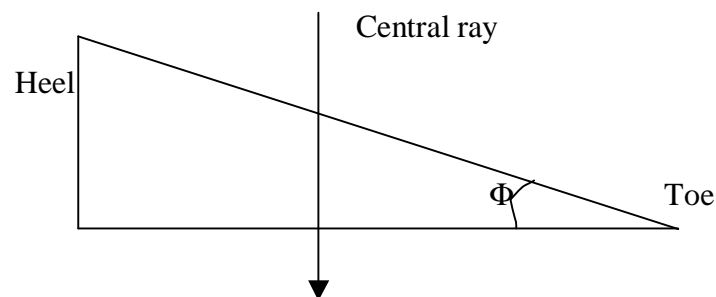


Figure 1- 4: A schematic of a wedge filter primarily designed to tilt the open beam isodose curves through an angle Φ . The heel transmits less of the initial beam and the toe transmits more.

1.2.3.2 2-D missing tissue compensators

2-D missing tissue compensators have been fabricated using both manual and automated systems. Although they are easy to make, they are deficient in catering for the variations in patient anatomy beyond two degrees of freedom, i.e. not all treatment machine movements are possible to reproduce viz. couch, collimator and gantry rotation. In these cases, the smallest rotation is normally ignored. This leaves a mismatch of the treatment fields that results into inhomogeneities of the dose in the treated area.

1.2.3.3 3-D missing tissue compensators

Automated systems like compute Rx-comp RTM have been used to fabricate 3-D missing tissue compensators. Although they are efficient and computerised, they require well-trained manpower and additional resources for their operation. These

systems are not only expensive to maintain, but require connectivity to a computed tomography (CT) based 3-D treatment planning system. Access to CT planning is often unavailable in many resource-constrained environments. In addition, most CT scanners have a field of view of approximately 50 cm. This does not permit imaging of patients that require a wider field of view, e.g. breast patients positioned on a tilted board.

The most sophisticated form of compensation available is the use of intensity-modulated fields (Dimitriadis and Fallone, 2002; Weston, June 2008). This requires CT-based 3-D inverse treatment planning. This is clearly the most manpower intensive and expensive option. Multileaf collimator (MLC) based compensators also do not produce continuous 3-D fluence intensity maps given the finite size of the individual leaves and often 3-D compensators are used instead.

1.3 Historical review of the methods of fabrication of missing tissue compensators and material used

Ellis *et al.*, (1959), Hall and Oliver (1960), Sundblom (1964) and Van de Geijin (1965) manually constructed 2-D missing tissue compensators using aluminium or brass blocks. They used a matrix of square columns corresponding to the irregular surface. This system aimed at reducing compensator size by incorporating geometric divergence if placed at a known distance from the patient's surface.

Gunilla *et al.*, (1989) describes a manual technique of fabrication of 2-D missing tissue compensators. Thin sheets of lead or brass with known attenuation are taped or glued together in a stepwise fashion to form a compensator as shown in figure 1-5. However, the system could only be used for cases where the patient's contour was slanting in a linear fashion.

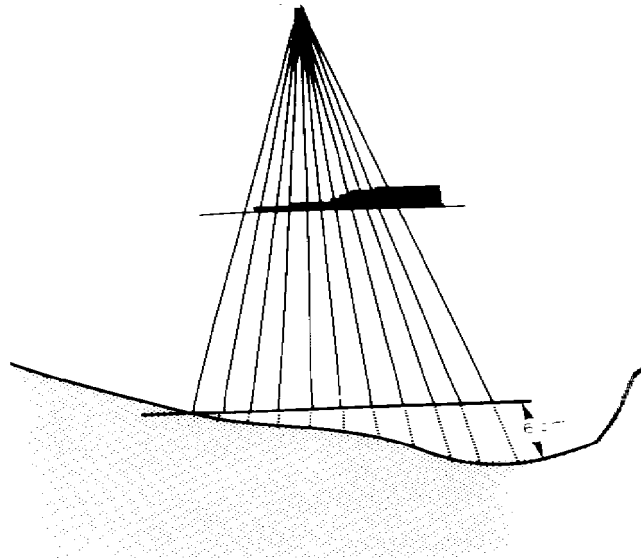


Figure 1- 5: A 2-D compensator constructed out of thin sheets of lead or brass in a stepwise fashion.

Beck *et al.*, (1971) and Boge *et al.*, (1974) describe a technique that used a Styrofoam cutter with a heating element or a routing tool to fabricate 2-D missing tissue compensators as shown in figure 1-6.

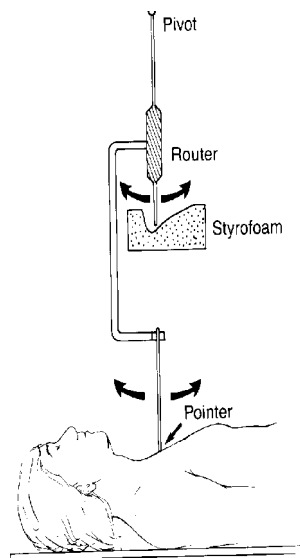


Figure 1- 6: A Styrofoam cutter fitted with a routing tool used by Boge, R. J to manually construct 2-D compensators.

The patient or a positive mould of the patient was placed at the treatment distance under a device that consisted of a pointer attached to a fixed pivot source point and

equipped with a router. The router was tightly mounted for stability at the same distance as the accessory holder of the designed treatment unit. A Styrofoam block was placed above the patient at the same distance from the pivot as the compensator would be mounted during the treatment. The central axis of the beam was marked for proper alignment of the compensator. A retractable pointer was moved along the patient's surface and the router milled out the Styrofoam to the shape of the missing tissue. The hollowed Styrofoam was then filled with a tissue equivalent material such as paraffin wax, and mounted during dose delivery in the treatment machine. This is performed for every treatment field.

The 3-D manual missing tissue compensator cutter system used in this research was a modification of that described by of Beck *et al.*, (1971) and Boge *et al.*, (1974). It was designed to allow for all movements of the teletherapy machine to permit 3-D missing tissue compensators to be fabricated with respect to all the degrees of freedom.

Khan *et al.*, (1968a, 1980b) used an apparatus with thin rods to duplicate the diverging rays of the treatment beam to fabricate 3-D compensators. The rods were moved freely in a rigid shaft along the diverging paths and were locked or released by a locking device. This apparatus was placed on the patient with the lower ends of the rods touching the skin. The rods were locked in place and their ends formed a reduced duplicate of the patient's skin surface topography as shown in figure 1-7.

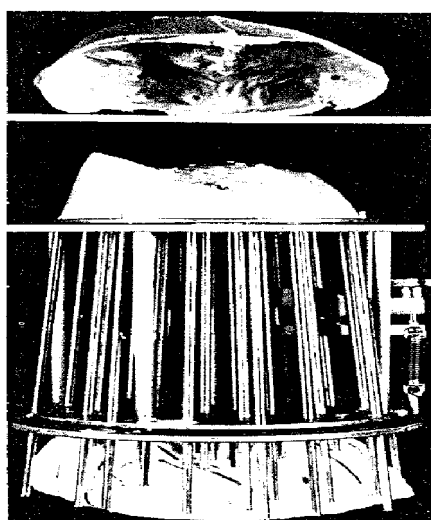


Figure 1- 7: An apparatus used by Khan to construct 3-D compensators in one piece.

Renner *et al.*, (1977) developed a system that used photogrammetry to obtain information about the patient's shape and size. The technique used a grid pattern projection of the field on the patient. The pattern that appeared as curved lines on the patient's irregular surface topography was photographed and the line pattern projected onto a graphics terminal of a computer for data entry. Using a computer algorithm, the 3-D topography of the patient's contour was reconstructed and the design of the tissue compensator calculated.

Shragge and Patterson (1981) described a computer driven compensator design and fabrication device. The system used irregular patient topography and inhomogeneities obtained from CT. The computer operated a Styrofoam cutter that cut a mould for 2-D or 3- D missing tissue compensators based on a dose calculation. The mould was filled with a tissue equivalent material and mounted in the treatment machine during dose delivery.

1.3.1 Linear attenuation coefficient

For a well collimated narrow beam of mono energetic photons incident on an absorber of variable thickness x , with a detector placed at a fixed distance from the source and at sufficient distance from the absorber for only the primary photons to be measured, the intensity $I(x)$ decreases exponentially with thickness of the absorber according to equation 1-1:

$$I(x) = I_0 e^{-\mu x} \quad \text{Equation 1- 1}$$

Where I_0 is the intensity with no attenuator and μ is the linear attenuation coefficient.

If x is measured in cm, μ has units cm^{-1} (Dendy and Heaton, 1999; Khan, 1994).

During CT scanning, a narrow beam of x-rays transmits a patient in synchrony with a radiation detector on the opposite side of the patient. A number of transmission measurements are taken at different orientations of the x-ray source and detector depending on the type of scanner and the distribution of attenuation coefficients within each layer is determined. Figure 1-8 shows different types of CT scanners.

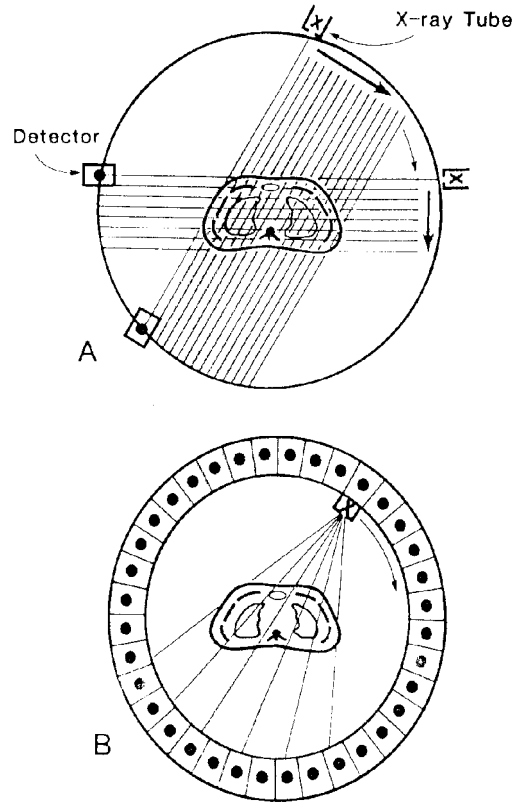


Figure 1- 8: Scan motion in CT, (a) shows an early design of a CT scanner with the x-ray source and the detector performing a combination of translational and rotational motion, (b) shows a modern CT scanner with the x-ray tube rotating within a stationary circular array of detectors (Khan, 1994).

CT number bears a linear relationship to the attenuation coefficient and it is related to the electron density (the number of electrons per cm^3) (Khan, 1994). The CT image is a reconstruction that is performed by a computer using mathematical algorithms. The reconstructed CT image represents various structures with different attenuation properties by assigning different grey scale levels to different attenuation coefficients. The reconstruction algorithms generate CT numbers, which are related to attenuation coefficients. These CT numbers are assigned such that -1000 represents air, $+1000$ represents hard bone and water is set at 0 . CT numbers normalised in such a manner are called Hounsfield numbers (H). This relationship is indicated in equation 1-2.

$$H = \frac{\mu_{\text{tissue}} - \mu_{\text{water}}}{\mu_{\text{water}}} \times 1000 \quad \text{Equation 1- 2}$$

Where μ is the linear attenuation coefficient.

1.3.2 Effect of linear attenuation coefficient of compensator filling material on the design of missing tissue compensators

In designing compensators, the aim is to ensure that the thickness of compensator material absorbs the equivalent amount of radiation as the thickness of tissue missing from the patient as shown in figure 1-9.

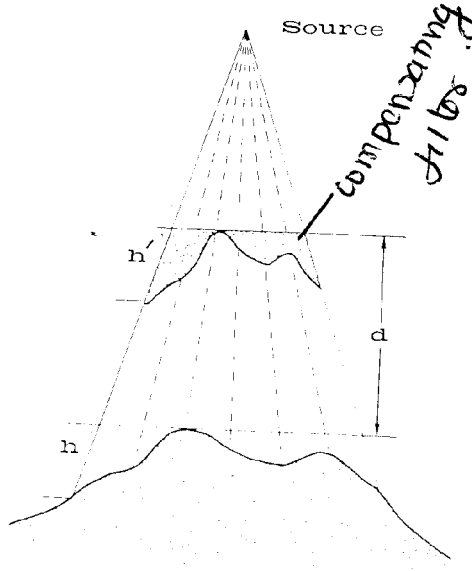


Figure 1- 9: Schematic representation of thickness h' of a tissue equivalent compensator in relation to the missing tissue thickness h along the same ray (Khan *et al.*, 1970).

The thickness ratio or the density ratio is defined as the required thickness of a tissue equivalent compensator along a ray (h') divided by the missing tissue thickness along the same ray (h) (Hall and Oliver, 1960). It can also be given by the reciprocal of the density of the compensator material as shown in equation 1.3.

$$\text{Thickness ratio or density ratio} = \frac{h'}{h} = \frac{1}{\rho_{\text{compensator}}} \quad \text{Equation 1- 3}$$

The linear attenuation coefficient (μ) of the missing tissue compensating material depends on the density (ρ) of the material. This is because the attenuation produced in the material of thickness (x) depends on the electron density. The relationship between μ and ρ gives the mass attenuation coefficient as shown in equation 1.4 (Khan, 1994).

$$\text{Mass attenuation coefficient} = \frac{\mu}{\rho} \quad \text{Equation 1- 4}$$

Thus the linear attenuation coefficient is used to compute the thickness ratio and is required for compensator design.

1.4 Statement of the problem

A patient's surface topography varies in 3-D. Teletherapy treatment machines have several degrees of freedom that should be reflected at the missing tissue compensator fabrication level. 1-D and 2-D missing tissue compensators have limitations in the degree of compensation for tissue deficits in treatment fields of highly irregular surface topographies. 3-D missing tissue compensators are clearly more effective but are currently fabricated using automated systems that are unavailable to developing countries.

A 3-D manual missing tissue compensator cutter system was designed as shown in figure 1-10. It was intended for manual fabrication of 3-D missing tissue compensators in patients that present with very irregular surface topographies at simulation.

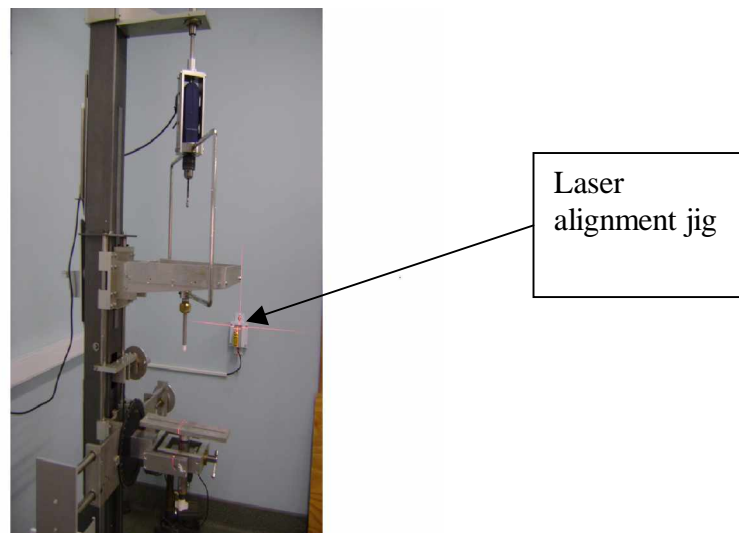


Figure 1- 10: The 3-D manual missing tissue compensator cutter.

The type of compensator filling material used affects the design of missing tissue compensator. Several materials could be used but their linear attenuation coefficients

must be known. Four materials (tin, River sand mix, Lincolnshire bolus and dental modelling wax) were tested in this work.

1.5 Aim of the study

The study aimed at commissioning the local 3-D manual missing tissue compensator cutter and the specific objectives were:

- i. To measure the linear attenuation coefficients of four materials (tin, River sand mix, Lincolnshire bolus and dental modelling wax) in a ^{60}Co teletherapy unit and medical linear accelerator photon beams of 6 MV, 15 MV and 18 MV nominal accelerating potential.
- ii. To select a tissue equivalent material to be used during 3-D missing tissue compensator fabrication.
- iii. To document the quality control procedures to be followed during missing tissue compensator fabrication.
- iv. To produce missing tissue compensators for typical breast and head and neck treatment fields.
- v. To evaluate the effectiveness of the fabricated 3-D missing tissue compensators during radiation treatment delivery.

CHAPTER TWO – METHODS AND MATERIALS

2.1 Determination of linear attenuation coefficient of materials

The linear attenuation coefficients (μ) of tin, River sand mix, Lincolnshire bolus and dental modelling wax were measured at four megavoltage photon beam energies: ^{60}Co (average energy of 1.25 MeV), 6 MV, 15 MV and 18 MV. A Theratron Equinox unit from MDS Nordion was used for the ^{60}Co measurements whereas Siemens Primus medical linear accelerators were used for the three high-energy photon beams.

7 cm \times 7 cm compensators of thicknesses 1 cm, 2 cm, 3 cm, 4 cm and 6 cm were produced in 30.5 cm \times 30.5 cm \times 10 cm pieces of low density Styrofoam. Each compensator was filled with one of the four materials. Double-sided tape was used to attach the compensator to a Perspex tray and these were screwed to a holder and mounted in the accessory holder of the teletherapy machine. The fixed accessory holder distances were 56.3 cm and 58.3 cm from the source of the linear accelerator and ^{60}Co treatment units respectively. The measured transmission factors (T_t) of the Perspex trays used were 0.964, 0.971, 0.981 and 0.981 for the ^{60}Co , 6 MV, 15 MV and 18 MV photon beams respectively.

Transmission measurements were made in a 30 cm \times 30 cm \times 30 cm water phantom. A cylindrical ionisation chamber (PTW 30013-1583) with an active volume of 0.6 cc and connected to an electrometer (PTW 10008-80378) was used. Measurements were made in a 10 cm \times 10 cm radiation field at 80 cm and 100 cm from the source for the ^{60}Co treatment unit and linear accelerator respectively. Measurements were done at depths (D) of 3 cm, 5 cm and 6 cm by changing the SSD but keeping the source detector distance constant. Figure 2-1 shows the experimental set-up.

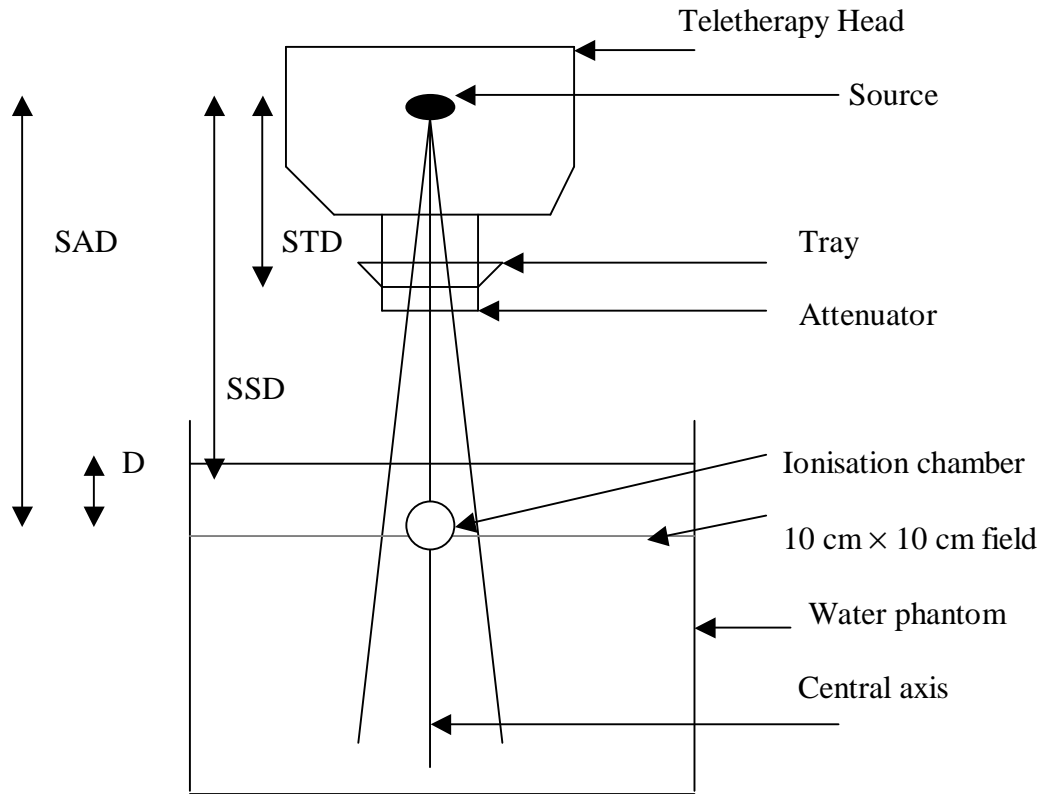


Figure 2- 1: Experimental set-up for the measurements of the linear attenuation coefficients where, SAD is the source-axis distance, SSD is the source-surface distance, STD is the source-tray distance (56.3 cm and 58.3 cm for linear accelerator and ^{60}Co treatment unit respectively) and D is the depth of measurement in the water phantom; 3 cm, 5 cm and 6 cm.

Transmission values for each beam were measured for each material, thickness and photon beam energy at each depth. Linear attenuation coefficients ($\mu_{\text{material}} \text{ cm}^{-1}$) were derived from the data using equation 2-1.

$$\mu_{\text{material}} = \frac{-\ln \left[\frac{\left(\frac{M_2}{M_1} \right)}{T_t} \right]}{X} \quad \text{Equation 2- 1}$$

Where, X is the thickness of the attenuator, T_t is the measured transmission factor of the perspex tray for every photon beam energy used, M_2 and M_1 are the chamber readings with and without the attenuator respectively.

2.2 Selection of a tissue equivalent material used in filling hollowed Styrofoam

2.2.1 CT numbers of materials

The CT numbers of tin, River sand mix, Lincolnshire bolus, dental modelling wax and water were measured.

A high-density polystyrene phantom of diameter 32.0 cm and thickness 15.0 cm was used. It contained 9 holes of different diameters at different positions in the phantom. Each of the five materials was sequentially placed into the central insert of the phantom of diameter 2.5 cm and 10.0 cm deep as shown in figure 2-2. This was done in order to avoid cross scatter if all materials were inserted in the different holes at the same time. The phantom was aligned in the CT scanner using a laser system as shown in figure 2-3. Measurements were done at 120 kV, 170 mA, and a slice thickness of 5 mm was used. Three sequential mid slices S_1 , S_2 , and S_3 were used to determine the average CT number.

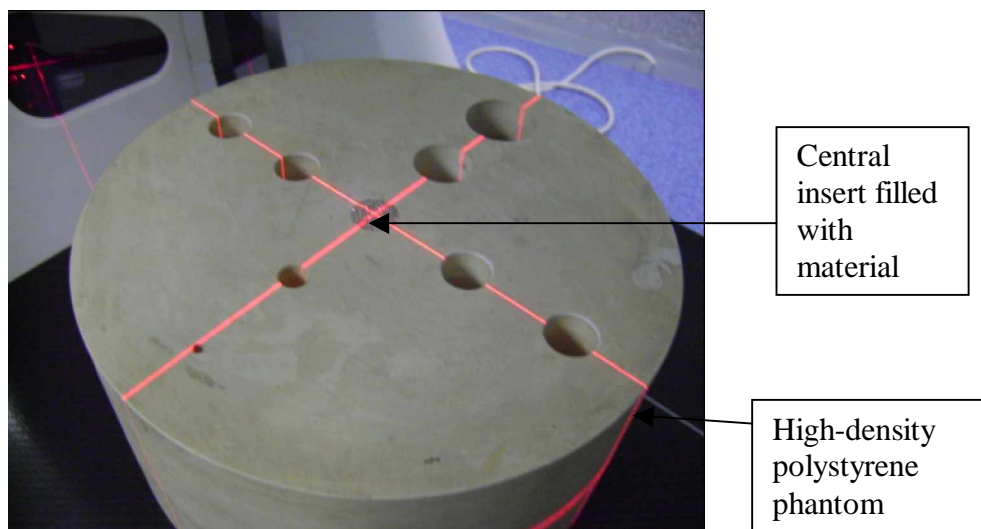


Figure 2- 2: High-density polystyrene phantom with central hole filled with material.

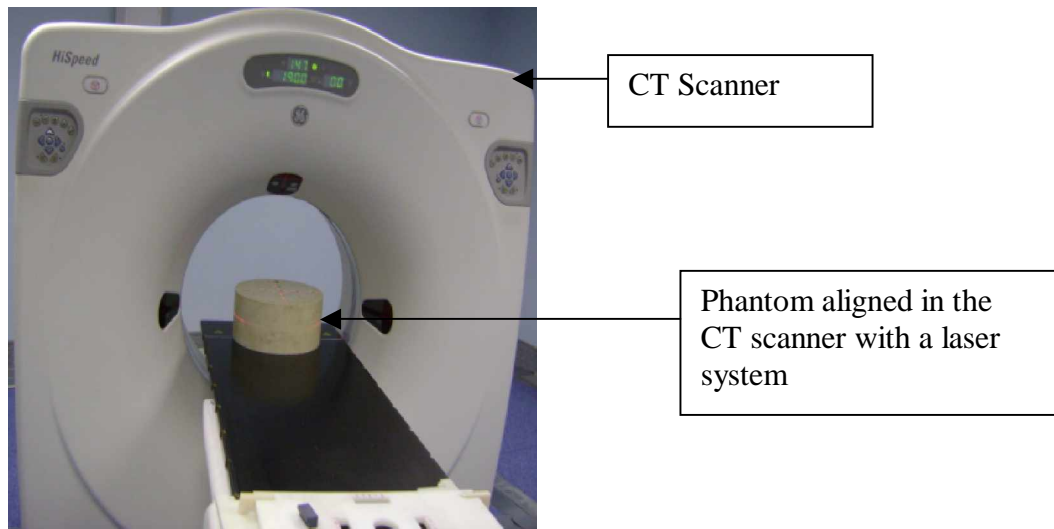


Figure 2- 3: Experimental set-up for the measurements of CT numbers of tin, River sand mix, Lincolnshire bolus, dental modelling wax, water and high-density polystyrene.

2.2.2 Densities of materials

The densities of tin, River sand mix, Lincolnshire bolus and dental modelling wax were measured using the water displacement method. Small quantities of each material were placed on a petri dish of mass 35.645 grams and their masses measured using a Precisa measuring beam balance. The measured materials were sequentially put in a 100 ml measuring cylinder containing a known volume of water. The displaced volumes were determined and the densities of each material calculated. The procedure was repeated three times and the average densities were calculated.

2.3 Irregular surface contouring and mould formation

2.3.1 Breast contouring and mould formation

Two breasts of different size, left breast size A and right breast size C, with labels AL and CR respectively, of the RANDOTM Alderson anthropomorphic phantom were used to represent typical patients. These were contoured using a simulator. Simulation films were taken for each showing the anatomical borders of typical supraclavicular and tangential fields as shown in figures 2-4 to 2-7. The simulation reference points, gantry angles, field length and isocentre depth for each treatment field were noted.

In addition, the couch rotations were calculated to perfect the match between the non-diverging supraclavicular field at its inferior border and the diverging tangential field

at its superior border. Table 2-1 shows the field parameters. The Supraclavicular fields were simulated using the SAD technique of 100 cm at a treatment depth of 3 cm. The tangential fields were simulated using an SSD of 100 cm. Solid wires were used to mark the borders of each breast tangential field as shown in figure 2-8.

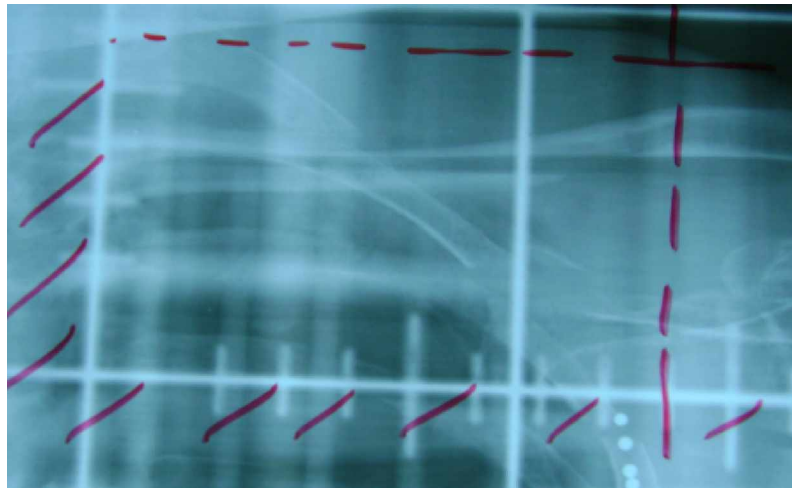


Figure 2- 4: Simulation film showing anatomical borders of supraclavicular field of RANDO™ Alderson anthropomorphic phantom's left breast (AL).

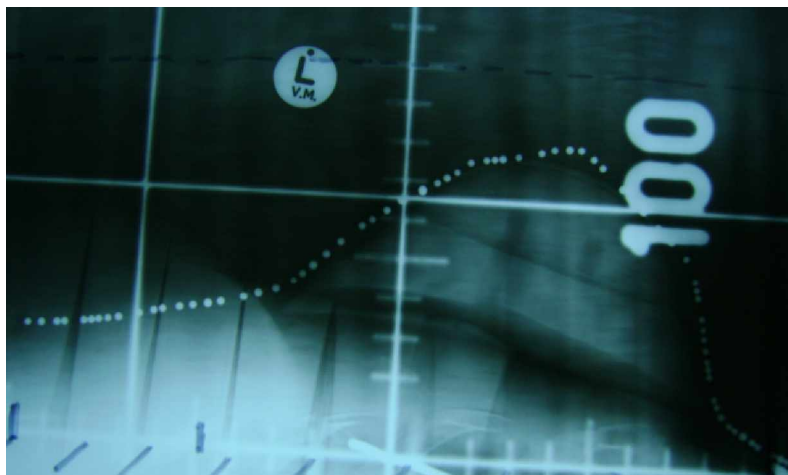


Figure 2- 5: Simulation film showing anatomical borders of tangential field of RANDO™ Alderson anthropomorphic phantom's left breast (AL).

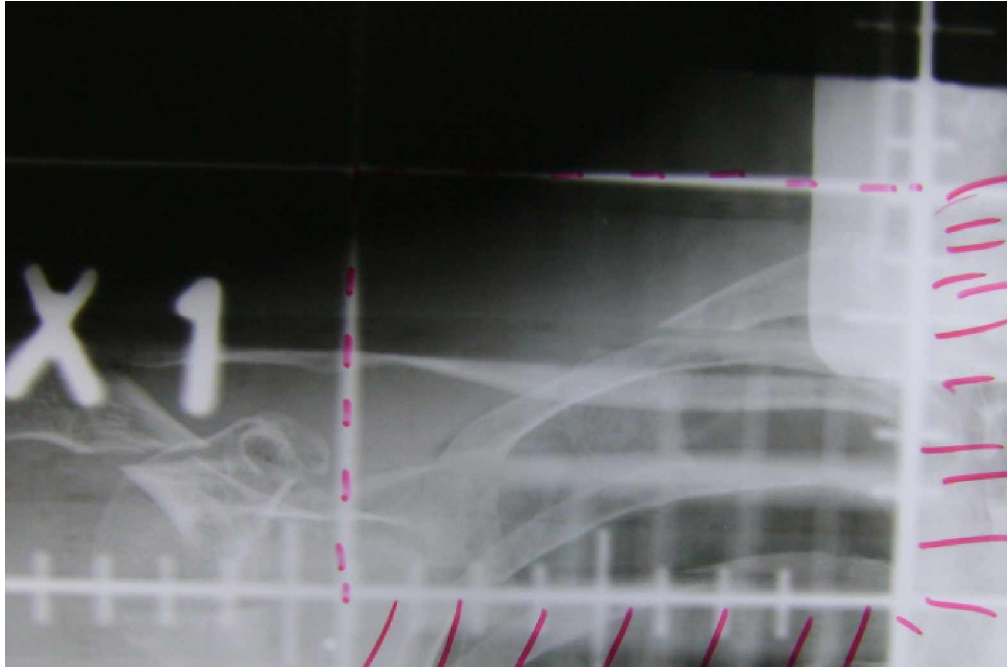


Figure 2- 6: Simulation film showing anatomical borders of supraclavicular field of RANDO™ Alderson anthropomorphic phantom's right breast (CR).

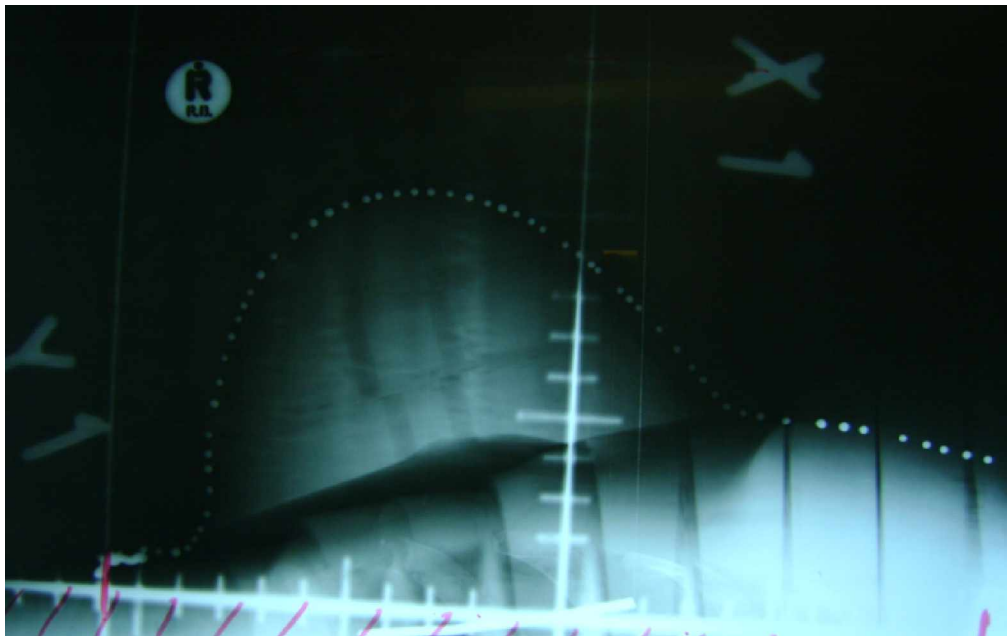


Figure 2- 7: Simulation film showing anatomical borders of tangential field of RANDO™ Alderson anthropomorphic phantom's right breast (CR).

Table 2- 1: Summary of reference points at simulation for left (AL) and right (CR) breasts

Reference points	Left breast (AL)	Right breast (CR)
(a) Supraclavicular field		
SSD (cm)	97.0	97.0
Depth of treatment (cm)	3.0	3.0
Gantry angle (degrees)	0	0
Technique of treatment	SAD	SAD
(b) Tangential field		
Separation of medial and lateral beam entry points (cm)	20.2	20.0
Depth of treatment (cm)	10.1	10.0
Set field size	10.0 cm × 19.7 cm	14.0 cm × 21.4 cm
Field size at a depth	11.0 cm × 21.7 cm	15.4 cm × 23.5 cm
SSD (cm)	100.0	100.0
Gantry for medial tangential field (degrees)	305	52
Couch rotation	6	6
Treatment technique	SSD	SSD

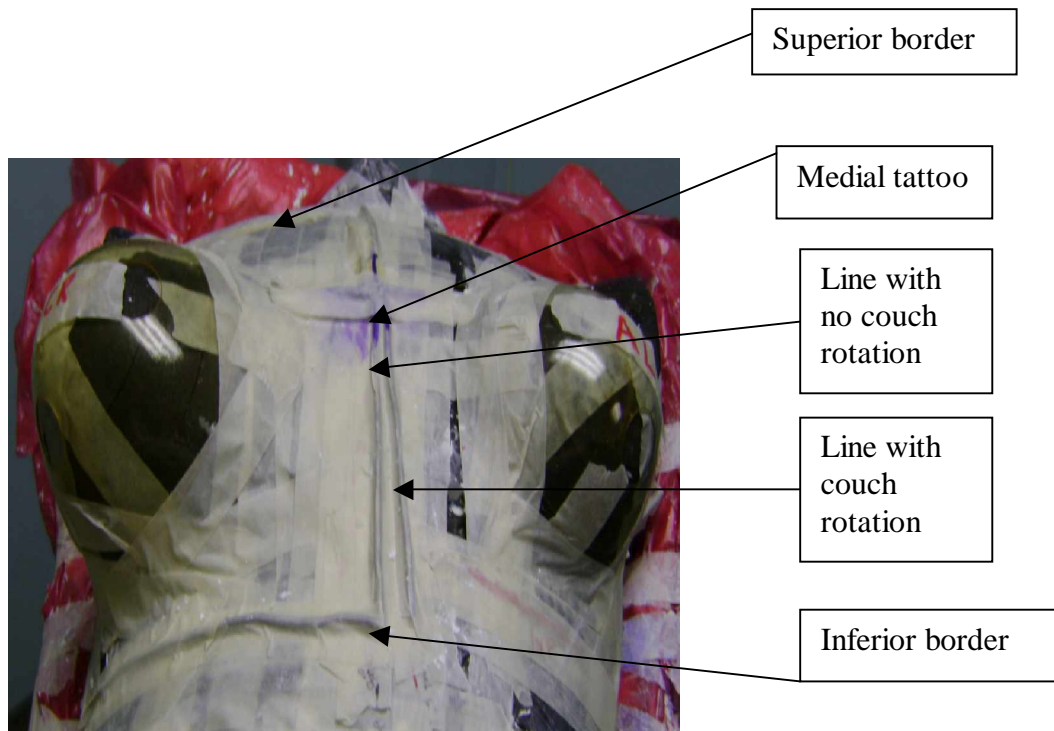
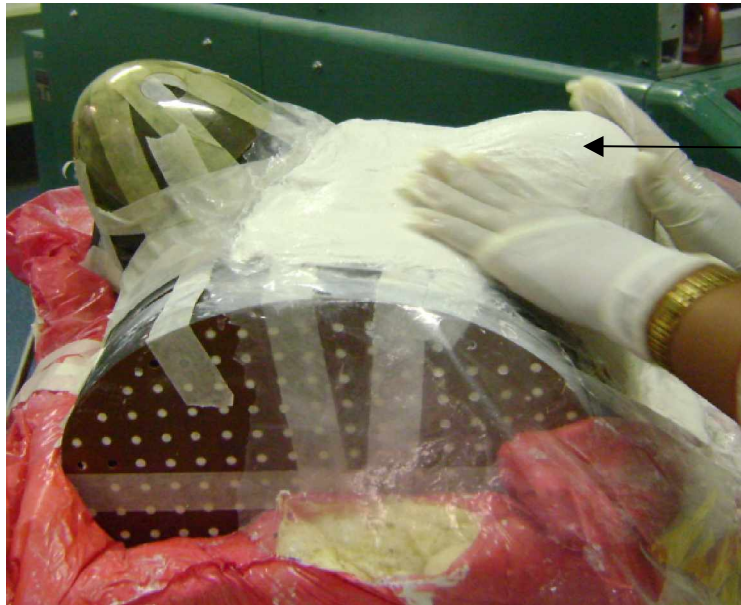


Figure 2- 8: Solid wires indicating the references for the right breast tangential field to be used in mould formation. (Similar references were applied to the left breast).

A Plaster of Paris (POP) mould was then made of each breast with reference to the solid wires as shown in figure 2-9. Labels were made on the POP mould showing its orientation on the treatment machine as shown in figure 2-10. These references guide the mounting of the mould during compensator fabrication. The POP moulds were left to dry for at least 12 hours before mounting for missing tissue compensator fabrication.



POP
bandages
used to make
a mould

Figure 2- 9: A mould of the left breast made using POP bandages.

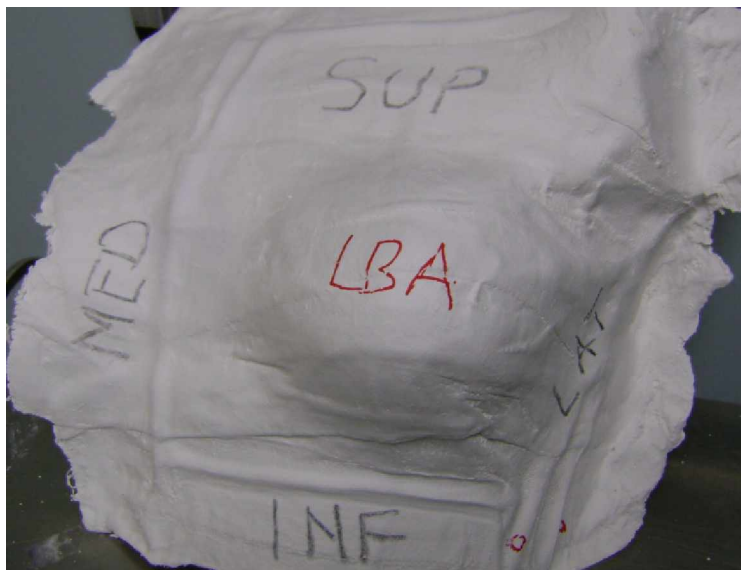


Figure 2- 10: Mould of the left breast indicating details of the breast type, orientation and reference markings of the field borders.

2.3.2 Head and neck contouring and mould formation

Similarly, typical head and neck fields were simulated on the RANDO™ Alderson anthropomorphic phantom. Simulation films were taken with typical anatomical borders of a right lateral field as shown in figure 2-11. The same borders and field size were reproduced for the left lateral field. The simulation reference points and treatment depths for parallel opposed right and left lateral treatment fields were noted and are recorded in table 2-2. Both fields were simulated using an SAD of 100 cm. Solid wires were used to mark the borders of each treatment field and the contour levels as shown in figure 2-12.

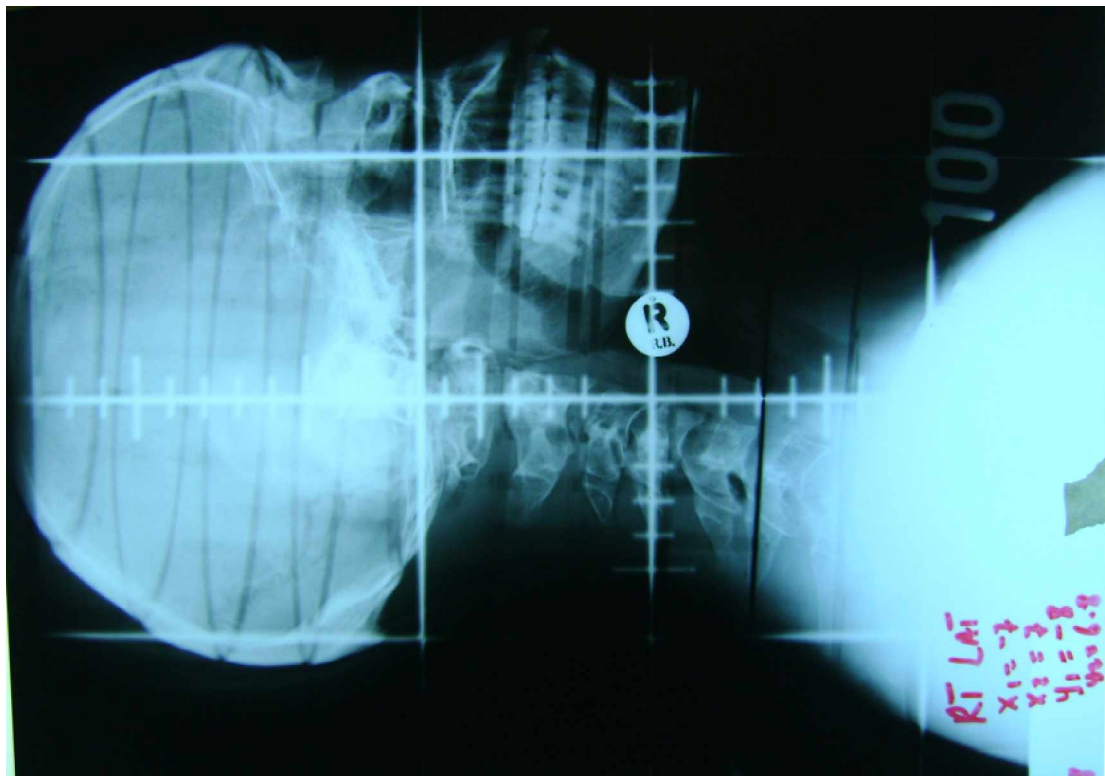


Figure 2- 11: Simulation film showing the anatomical borders of the right lateral field of RANDO™ Alderson anthropomorphic phantom's head and neck.

Table 2- 2: Summary of reference points at simulation for right and left lateral treatment fields for head and neck.

Reference points	Right lateral head and neck	Left lateral head and neck
SSD (cm)	94	94
Depth of treatment (cm)	6.0	6.0
Gantry angle (degrees)	270	90
Technique of treatment	SAD	SAD

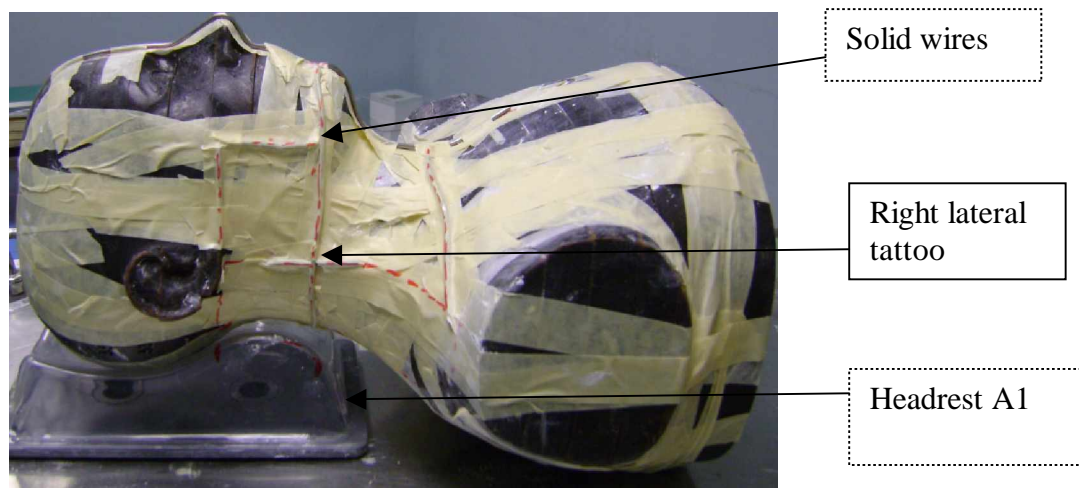


Figure 2- 12: Solid wires indicating the references for the right lateral head and neck field to be used in mould formation. (Similar references were applied to the left lateral field).

Two POP moulds (left and right) were made according to the markings as shown in figure 2-13. Orientation labels were made on the moulds and the wire traces appeared on the POP mould as shown in figure 2-14. These references guide the mounting of the mould during compensator fabrication. The POP moulds were left to dry for at least 12 hours before mounting for missing tissue compensator fabrication.



Figure 2- 13: A mould of the left lateral head and neck made out of POP bandage.

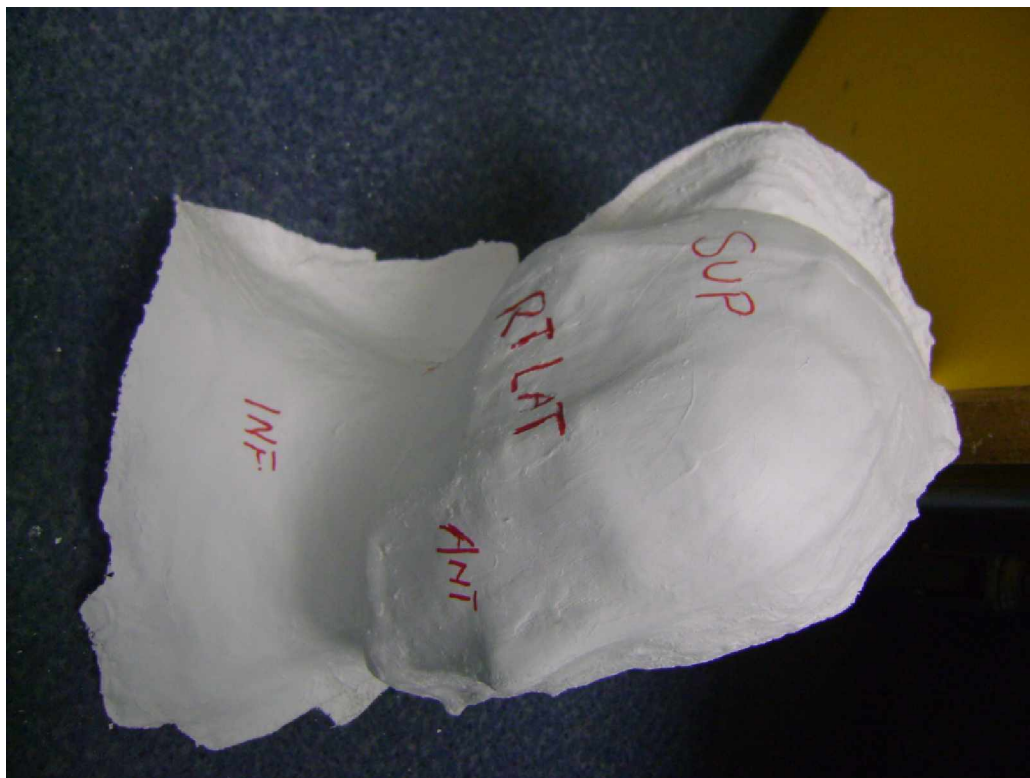


Figure 2- 14: A mould of the right lateral head and neck indicating orientation and reference markings of the field borders.

2.4 Quality control procedures for mould alignment and 3-D missing tissue compensator fabrication at the 3-D manual missing tissue compensator cutter

2.4.1 General approach and quality control of the 3-D manual missing tissue compensator cutter

The general layout of the 3-D manual missing tissue compensator cutter is shown in figure 2-15.

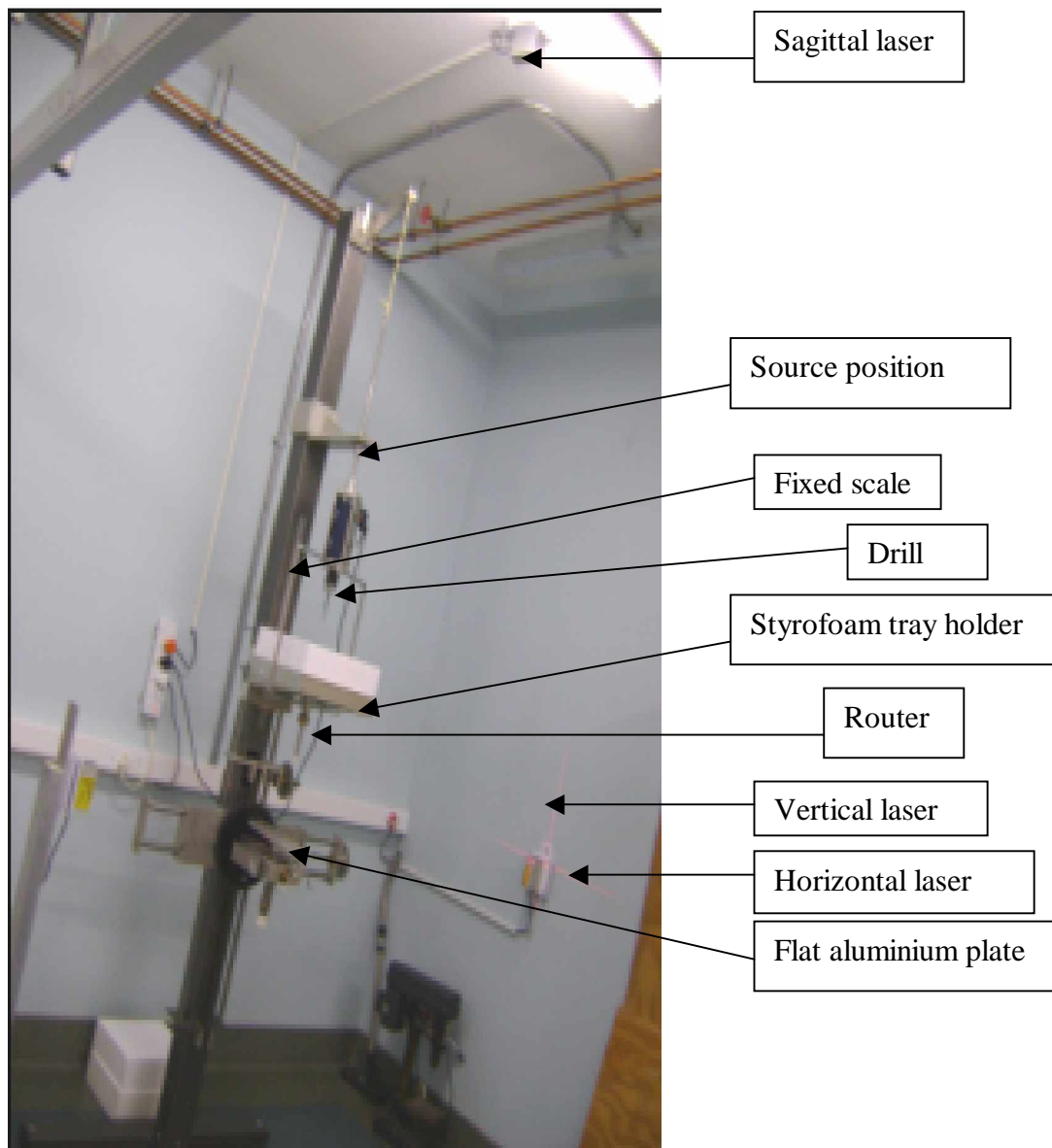


Figure 2- 15: Design of the 3-D manual missing tissue compensator cutter.

A standard size of Styrofoam (30.5 cm × 30.5 cm × 10.0 cm) fits into the Styrofoam tray holder. The drill bit was 6 cm long and routers of different length were available as shown in figure 2-16.



Figure 2- 16: Routers of different length.

The orthogonal laser system was set to meet at a point (I), a distance of 100 cm from the source position (S), which corresponded to the SAD of the linear accelerator. The distance from the source position (S) to the top of the Styrofoam (T) was set to 56.3 cm using the fixed scale. This corresponded to the source to tray distance of the linear accelerator. The distance from the top of the Styrofoam (T) to the laser was set to 43.7 cm using a demountable portable tape measure shown in figure 2-17 which fitted into the Styrofoam tray holder.



Figure 2- 17: Demountable portable tape measure used to measure distance IT.

Two jig systems were designed for easy mounting of breast and head and neck moulds respectively on the flat aluminium plate as shown in figure 2-18. The machine had six movements L, M, N, O, P and Q that permitted all the movements of the treatment machine, correct mounting of the mould and 3-D missing tissue compensator fabrication. Figure 2-19 shows the movements L, M, N, O, P and Q.

It also illustrates the distances SI, ST and TI. Corresponding movements are indicated at the treatment machine in figure 2-20. The arrows indicate the direction of each movement.

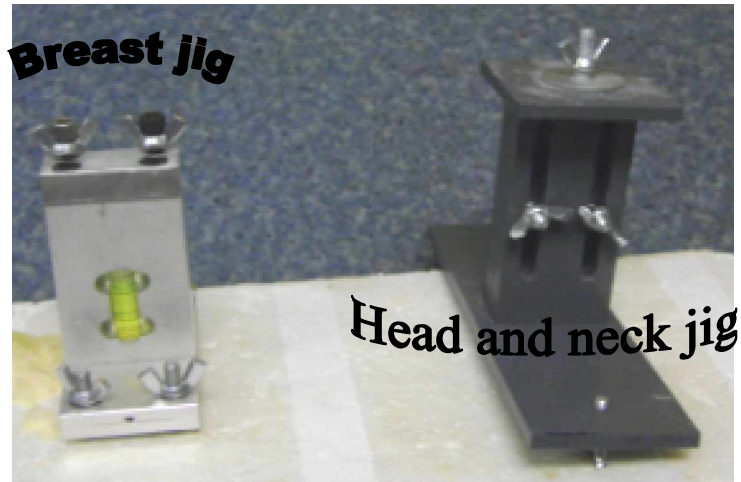


Figure 2- 18: Jig systems for mounting the breast and head and neck POP moulds onto the cutter.

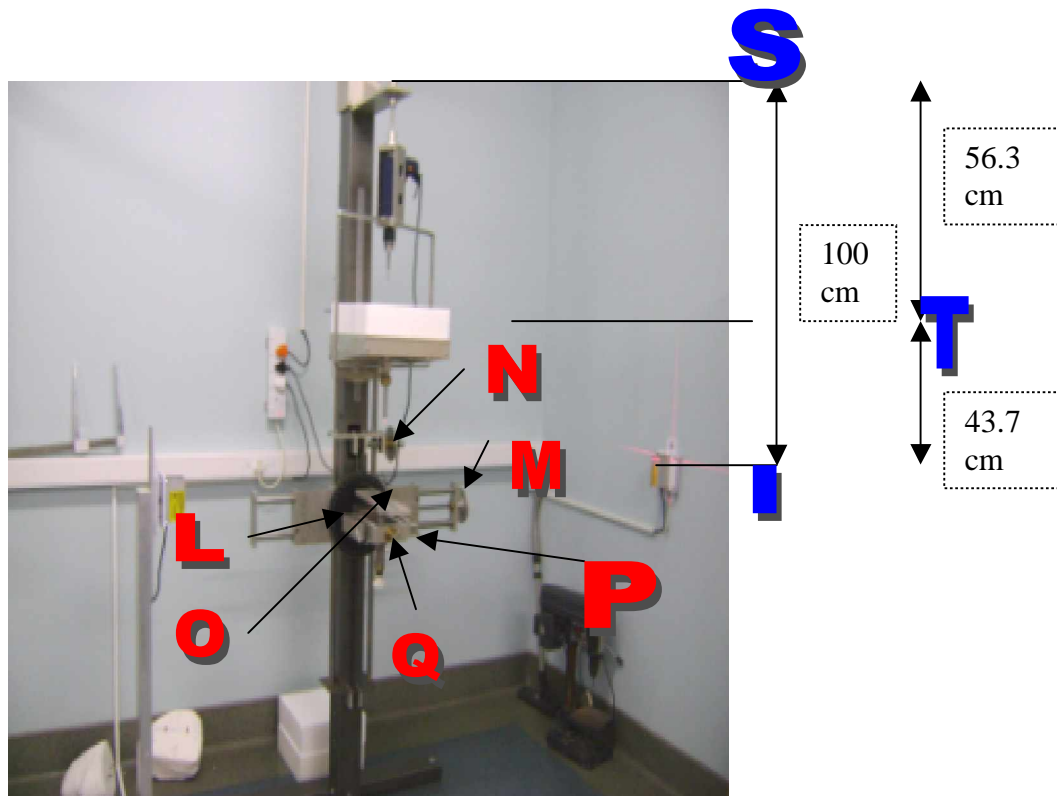


Figure 2- 19: Distances and movements used for correct mould mounting and 3-D missing tissue compensator fabrication. (L - Gantry, N- Lateral, M- Vertical, O- Longitudinal, P- Vertical laser and point of interest on the mounted POP mould, Q- Sagittal laser and point of interest on the mounted POP mould).

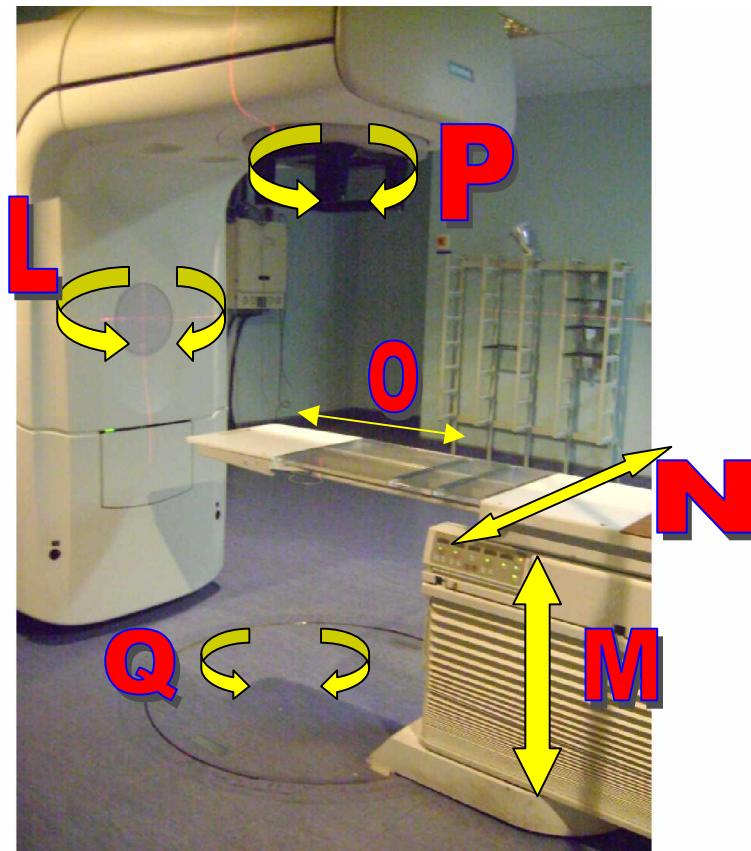


Figure 2- 20: Movements L, N, M, O, P and Q of the cutter as reflected by similar movements of the treatment machine. The arrows show the direction of each movement.

2.4.2 Manufacture of breast compensators

A straight metal rod of about 3 mm diameter was positioned through the medial and lateral reference marks of the dry POP breast mould. This was mounted onto the breast jig system as shown in figure 2-21. The rod was to ensure that the entrance and exit of the tangential fields remained in line with the central axis of the source and perpendicular to the floor during breast compensator fabrication.

Movement L in figure 2-19 was used to set the correct beams-eye-view. For the breasts, the medial and lateral tangential compensators were fabricated at opposing angles determined by L. For each angle L, the jig holding the mould was mounted on the flat aluminium plate of the cutter as shown in figure 2-22. The superior and

inferior orientation of the borders was noted. The references to the longitudinal, lateral and vertical (anterior/ posterior) movements were used to completely align the mould.

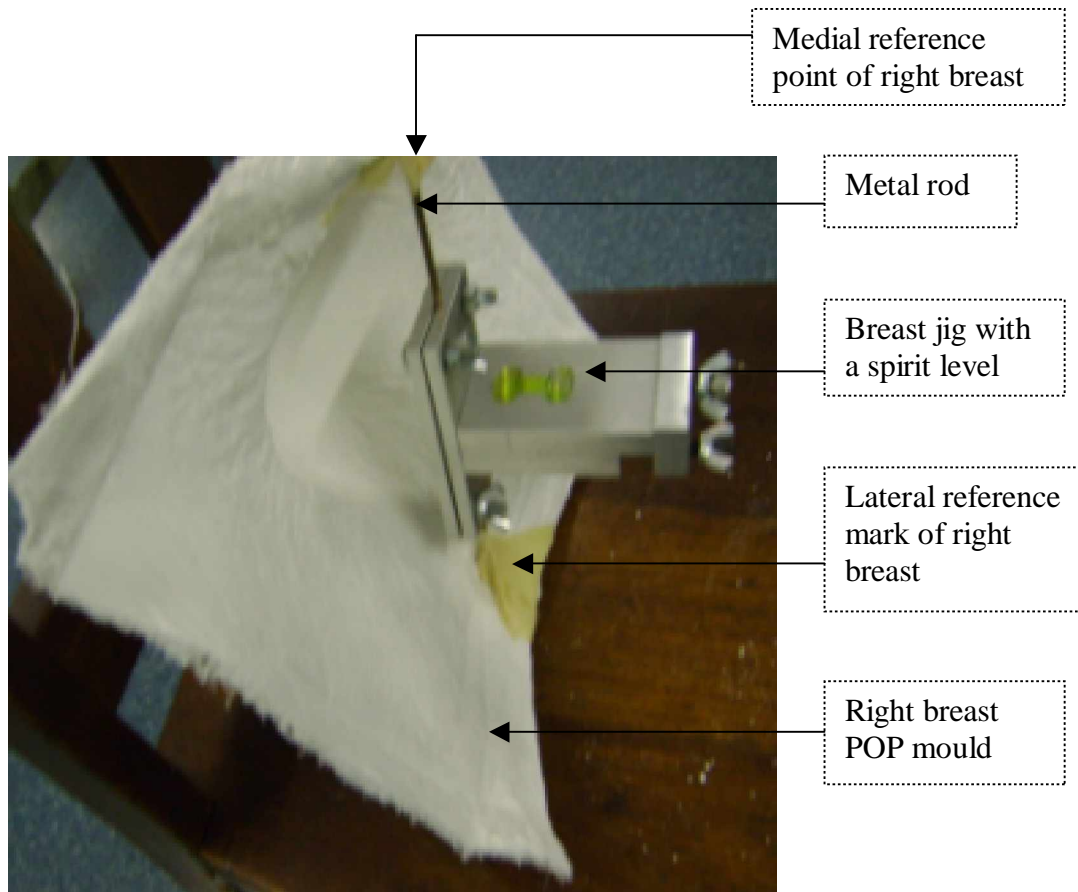


Figure 2- 21: Breast mould mounted on the breast jig system using a straight metal rod.

In figure 2-19, the beam entry point on the mould was placed 100 cm from the source position (S). Movement Q was used to align the external laser through the reference on the mould that showed the superior border obtained with couch rotation. Another metal rod was used to fix this position of the mould. Movement P was used to align the vertical laser through both opposing beam entry points, i.e. the entrance and exit of the tangential fields. The spirit level fixed in the breast jig system confirmed this set-up.



Figure 2- 22: Alignment of the breast mould at the cutter for the left lateral tangential treatment field during compensator fabrication.

The Styrofoam was centred and placed in the Styrofoam tray holder. The field borders of the mould were traced onto the Styrofoam as shown in figure 2-23. The drill bit was then moved along the marked field borders while the router was moved along the mould as shown figure 2-24. The drilled Styrofoam ultimately revealed the contour of the patient in 3-D as shown in figure 2-25. The contour was filled with Lincolnshire bolus, mounted onto the Perspex tray as shown in figure 2-26 and then tested for its effectiveness during treatment delivery. The process was repeated for both breast fields.

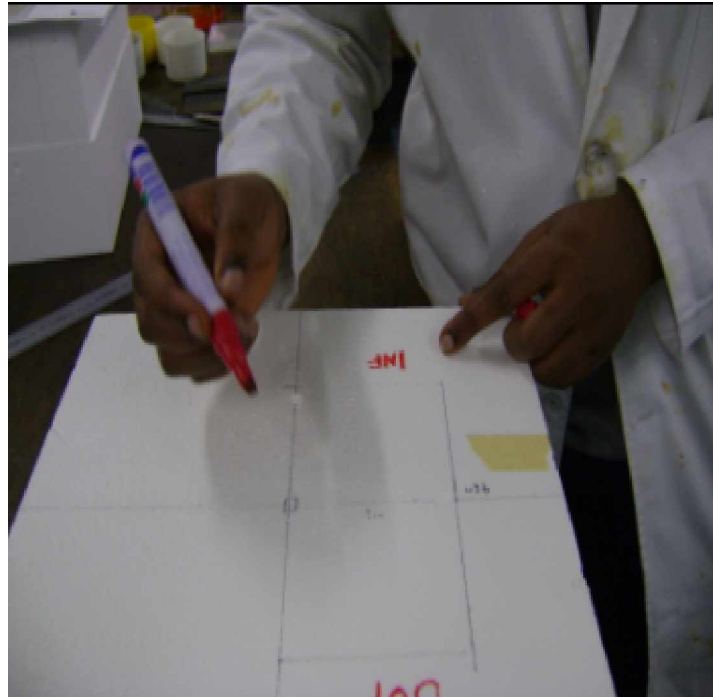


Figure 2- 23: Field borders of the treatment area marked onto the Styrofoam.



Figure 2- 24: Fabrication of hole into Styrofoam at the cutter.

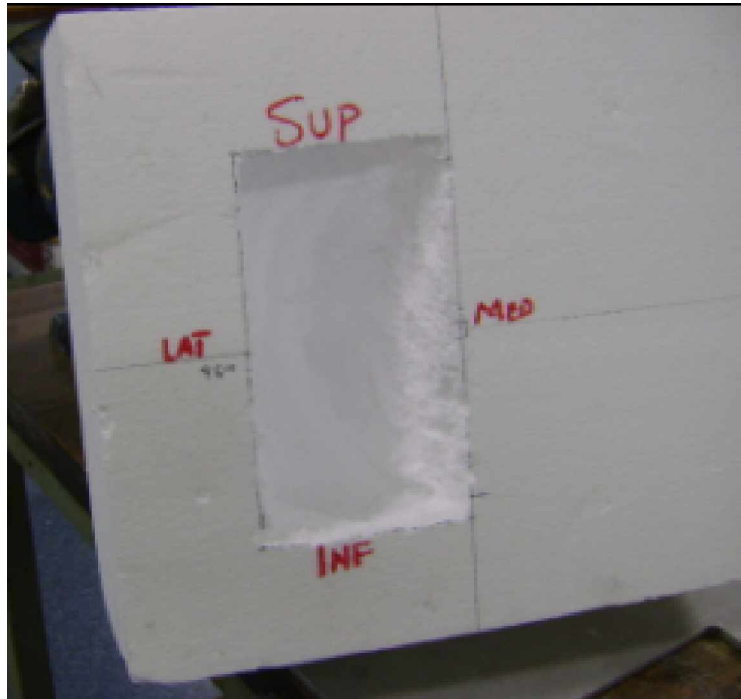


Figure 2- 25: Styrofoam milled according to the contours of the right breast medial tangential field.

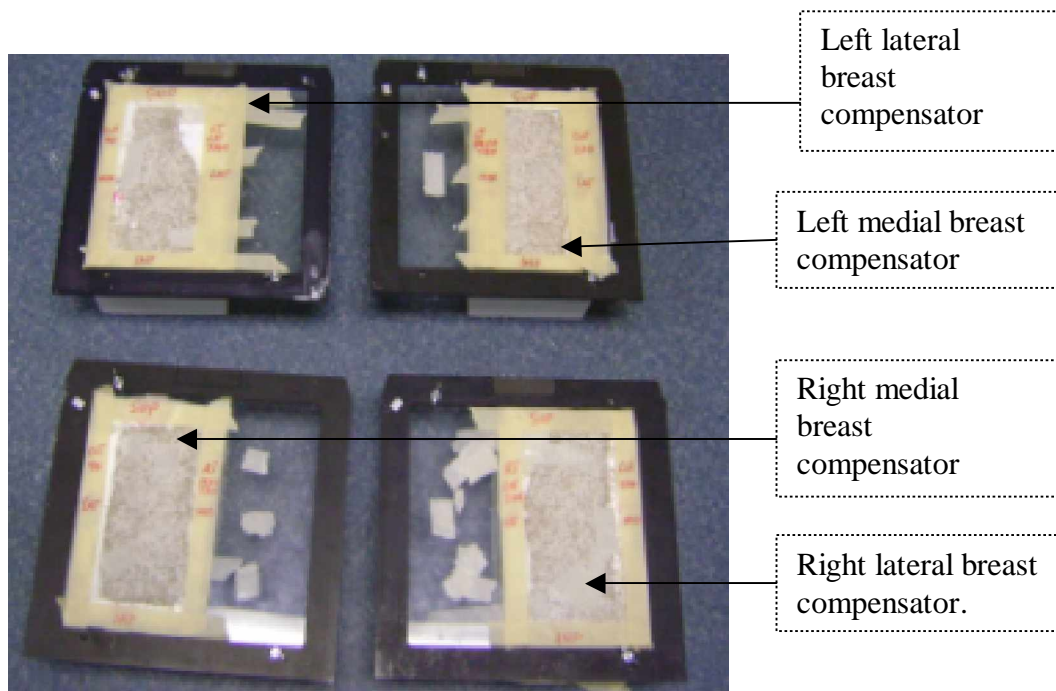


Figure 2- 26: Styrofoam filled with Lincolnshire bolus to form 3-D missing tissue compensators for both the lateral and medial tangential fields of the left and right breasts, mounted on the Perspex trays.

2.4.3 Manufacture of head and neck compensators

In figure 2-19, movement L was used to set the gantry angle for jig mounting and compensator fabrication using the dry POP mould. The right and left lateral compensators were also fabricated in the vertical position.

Movements O, P and Q were used to align the head and neck jig system on the flat aluminium plate such that the jig was in line with the central axis and perpendicular to the floor as shown in figure 2-27. The mould was mounted onto the jig, with the centre of the field (right and left lateral references) at a distance of 100 cm minus the depth from the source (S) (the point where the sagittal and axial references met). This corresponded to the set-up at the simulator as shown in figure 2-28. The lateral movement N and anterior/posterior movement M were used to achieve the alignment. The superior-inferior orientation was noted. A nut was used to fix the mould onto the jig.

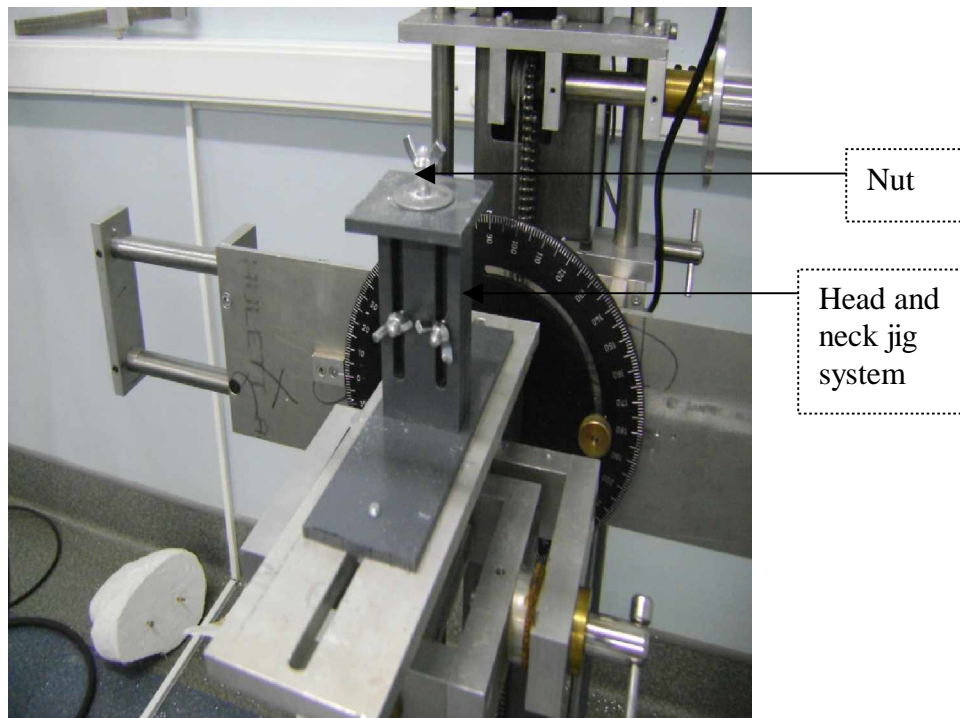


Figure 2- 27: Head and neck jig mounted on the flat aluminium plate.



Figure 2- 28: A POP mould of the left lateral head and neck treatment field mounted on the head and neck jig system.

The Styrofoam was centred and placed in the Styrofoam tray holder. The field borders of the mould were traced onto the Styrofoam using the drill bit and the router similar to the procedure used for the breast. The drill was moved along the marked field borders of the Styrofoam while the router was moved along the mould. The drilled Styrofoam reflected the contours of the patient. Again this was filled with Lincolnshire bolus, mounted on the Perspex tray and then tested for its effectiveness during treatment delivery.

2.5 Film dosimetry to determine effectiveness of fabricated 3-D missing tissue compensators

Negative moulds of the left breast, right breast and head and neck were filled with POP powder to form positive moulds (casts). The casts were left for at least 3 days and then stripped of the POP bandages such that the simulation markings appeared on each cast. The breast casts were bisected perpendicular to the mid plane between the medial and lateral tangential beam entrance points. The head and neck cast was bisected sagittally through the isocentric plane. Figure 2-29 shows the casts. These were used at the treatment machine to test the effectiveness of the fabricated 3-D missing tissue compensators.

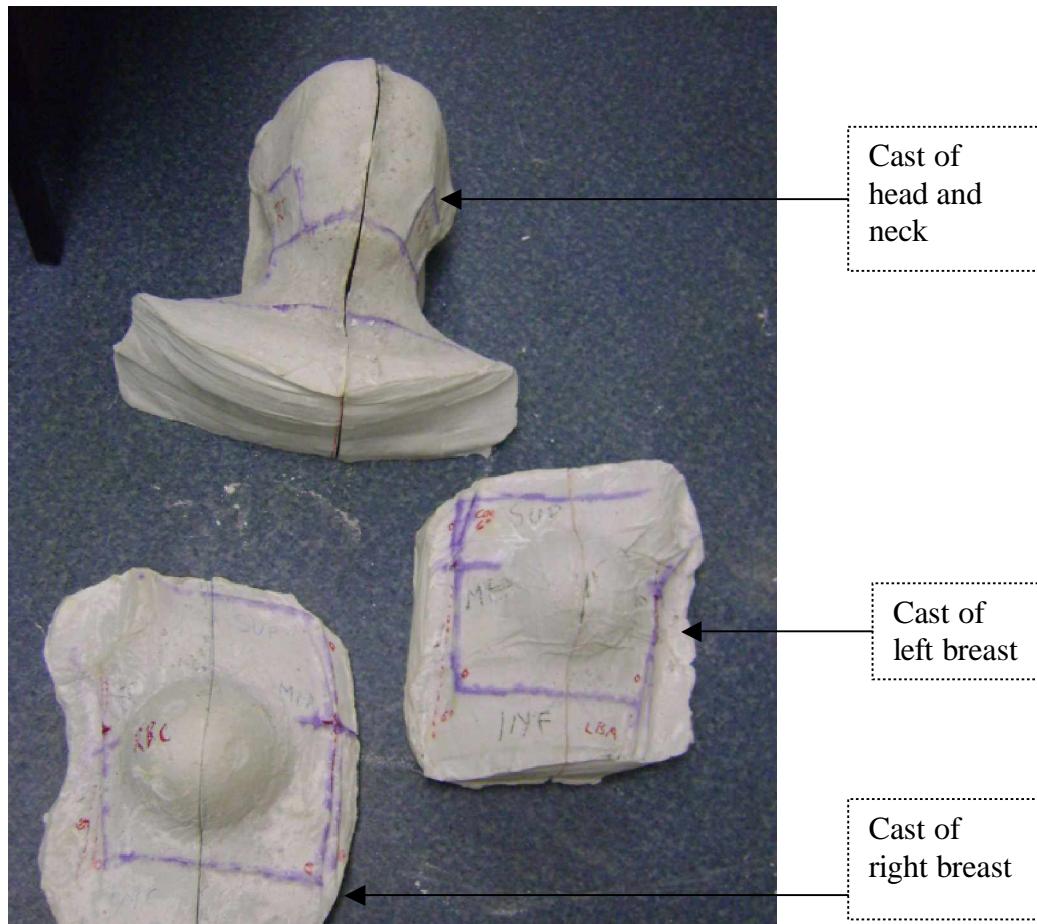


Figure 2- 29: Bisected casts of left breast, right breast and head and neck.

The treatment monitor units for the breast phantom were calculated for the treatment fields as open fields, a 30-degree anterior wedge pair and using the fabricated 3-D missing tissue compensators at 6 MV energy beam from a linear accelerator using the simulated field parameters as shown in table 2-3. A total dose of 50 cGy to the mid plane was used for each breast, using a contribution of 25 cGy from each tangential field. The same procedure was used for the head and neck fields but the total dose at midline was 40 cGy with a contribution of 20 cGy from the left and right lateral field each and a 15-degree inferior wedge pair was used instead. The doses of 25 cGy and 20 cGy were used to allow adequate variation in the optical density of the film and to avoid saturation at 1 Gy. The bisected cast was aligned according to the simulation, double emulsion 1 Gy Kodak X-OmatV verification film was placed into the bisected cast and exposed according to the calculated monitor units. Figures 2-30 to 2-36 show the experimental set-up of the fields at the treatment machine.

Table 2- 3: Calculated monitor units (mu) to deliver the same dose using different beam modifiers in the treatment field.

(a) Left breast (AL)		
Beam modifier	Left medial tangential	Left lateral tangential
Open field	37 mu	37 mu
30 degree real wedge field	69 mu	69 mu
3-D compensator field	38 mu	38 mu
Gantry angle (degrees)	274	94
Collimator (degrees)	0	0
(b) Right breast		
Beam modifier	Right medial tangential	Right lateral tangential
Open field	35 mu	35 mu
30 degree real wedge field	67 mu	67 mu
3-D compensator field	36 mu	36 mu
Gantry angle (degrees)	84	264
Collimator (degrees)	0	0
(c) Head and neck		
Beam modifier	Right lateral	Left lateral
Open field	21 mu	21 mu
15 degree virtual wedge field	21 mu	21 mu
3-D compensator field	22 mu	22 mu
Gantry angle (degrees)	270	90
Collimator (degrees)	0	0

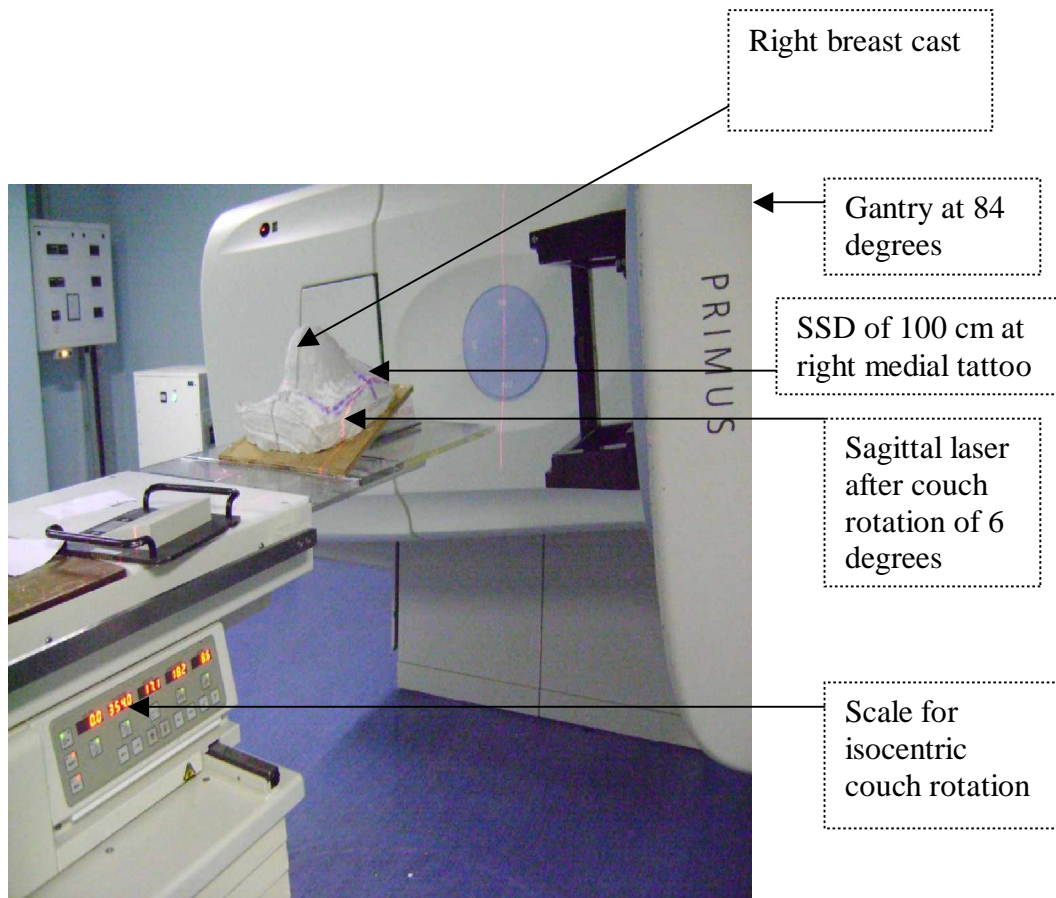


Figure 2- 30: Experimental set-up of the right breast cast at the treatment machine for the right medial tangential field with the gantry such that the back-pointer aligned with the right lateral plane.

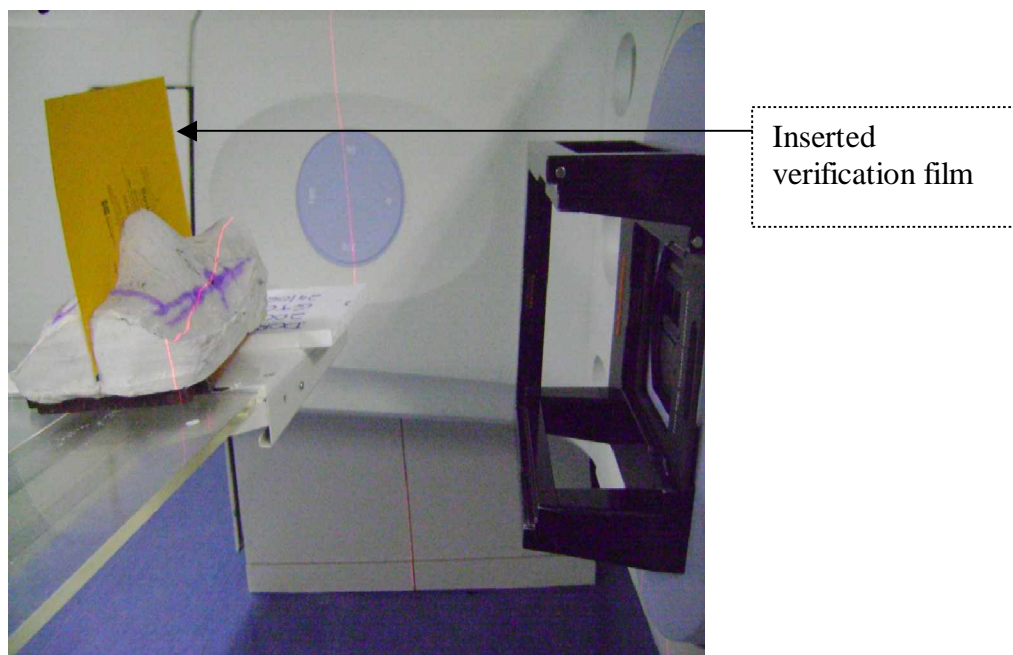


Figure 2- 31: Film exposed with an open field for the left lateral tangential field of the left breast.

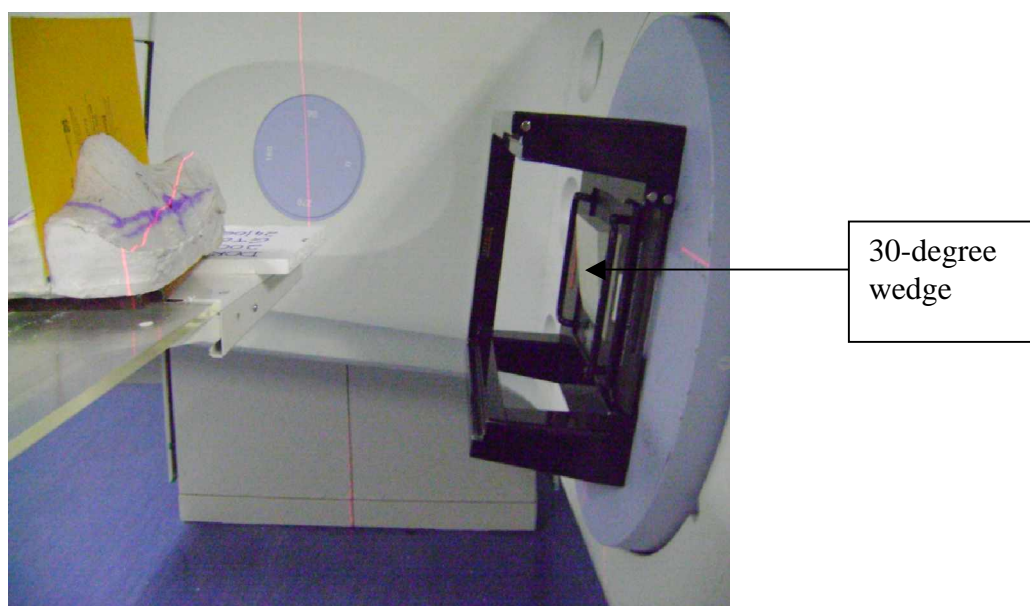


Figure 2- 32: Film exposed with a 30-degree wedge in the treatment field of the left lateral tangential field of the left breast.

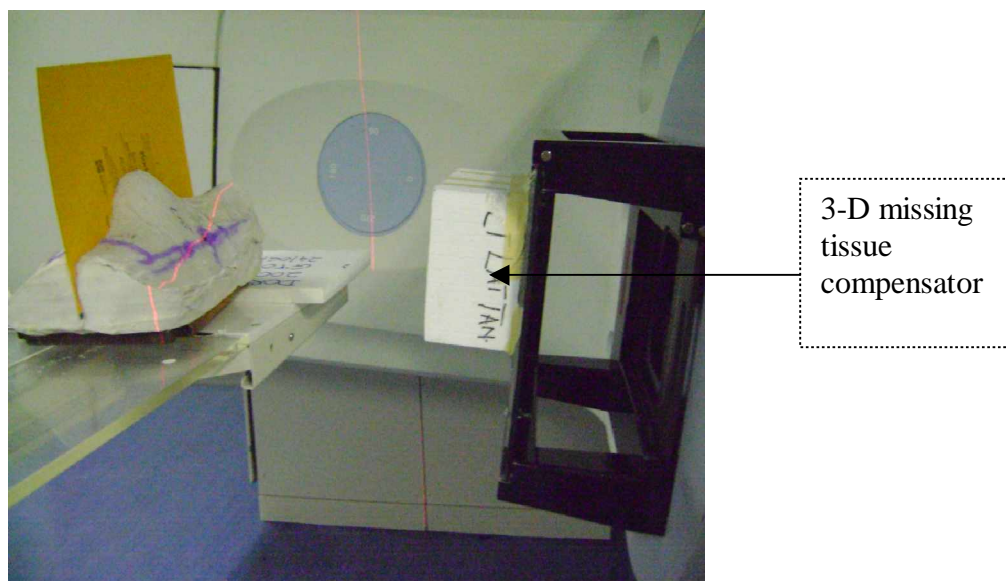


Figure 2- 33: Film exposed with a manually fabricated 3-D missing tissue compensator in the treatment field of the left lateral tangential.

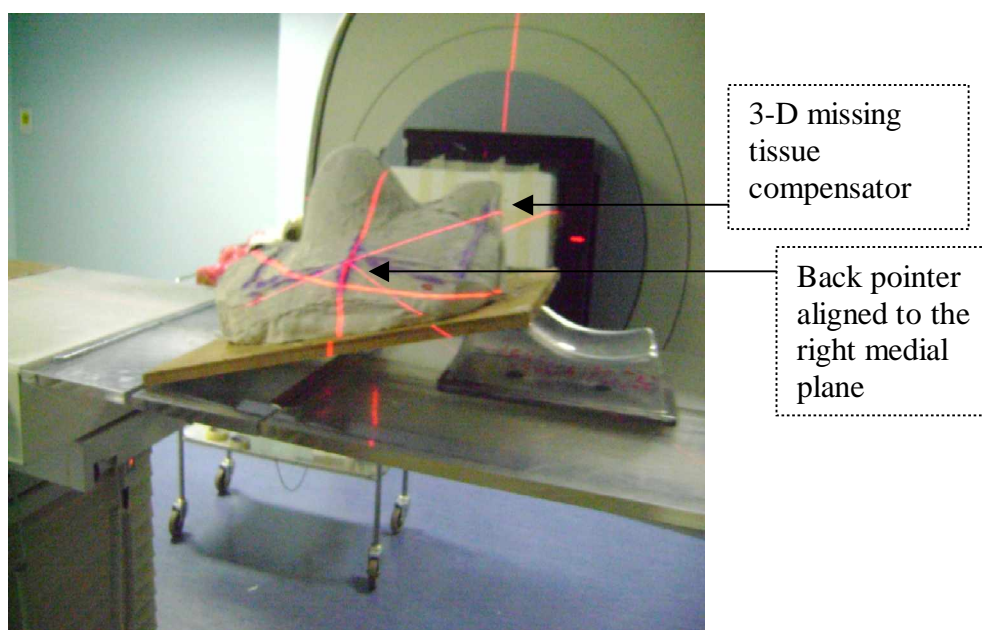


Figure 2- 34: Experimental set-up with 3-D manually fabricated missing tissue compensator in the treatment field of the right lateral tangential with the back pointer aligned to the right medial plane.

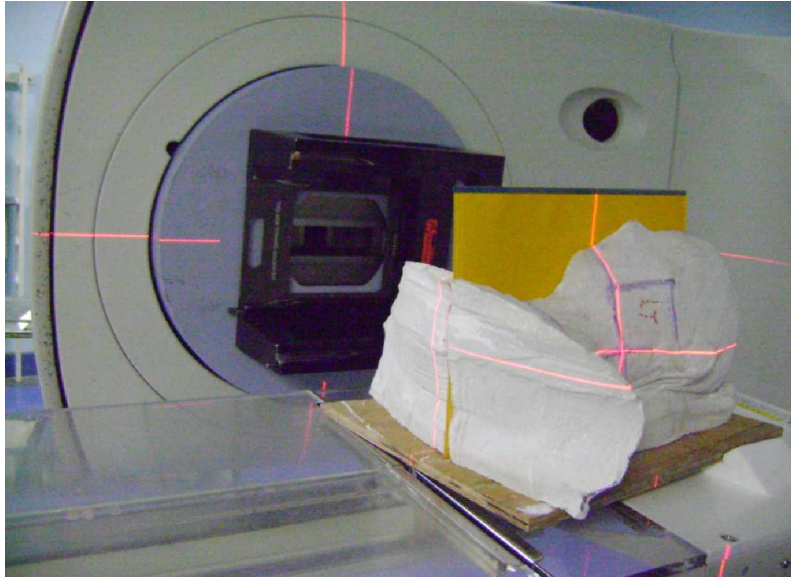


Figure 2- 35: Film exposed in the open right lateral treatment field of head and neck.

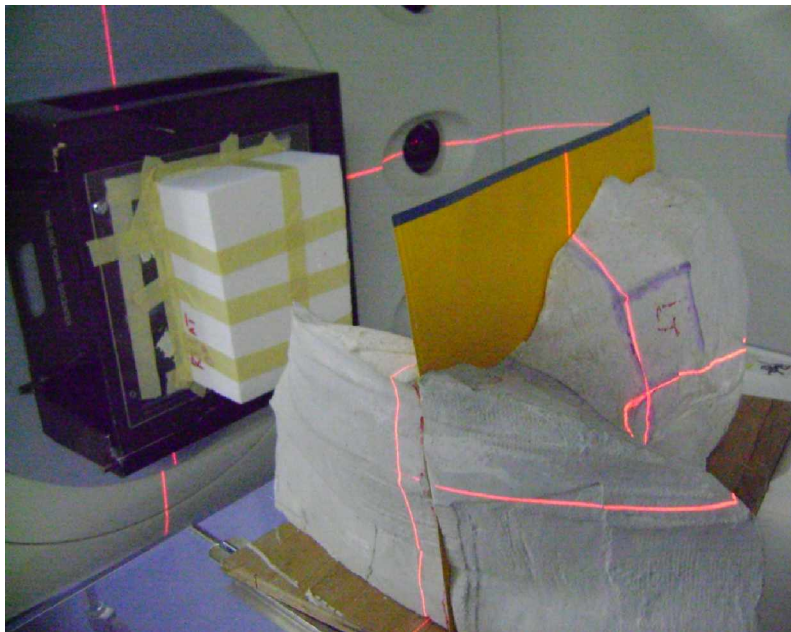


Figure 2- 36: Film exposed with 3-D missing tissue compensator in the right lateral treatment field of head and neck.

A densitometer (PTW T52001-N3968) was used to analyse the relative dose uniformity of the exposed films. The same anatomical points were used for each treatment field.

CHAPTER THREE – RESULTS AND DISCUSSION

3.1 Results of linear attenuation coefficient

The measured values of the linear attenuation coefficients for tin, River sand mix, Lincolnshire bolus and dental modelling wax as obtained using equation 2.1 are shown in figures 3-1 to 3-4. The experiment was performed once. The error bars represent the overall deviation in the measured values of linear attenuation coefficient from the readings with a maximum of $\pm 0.001 \text{ cm}^{-1}$. No error bars were indicated with zero error in the measured values.

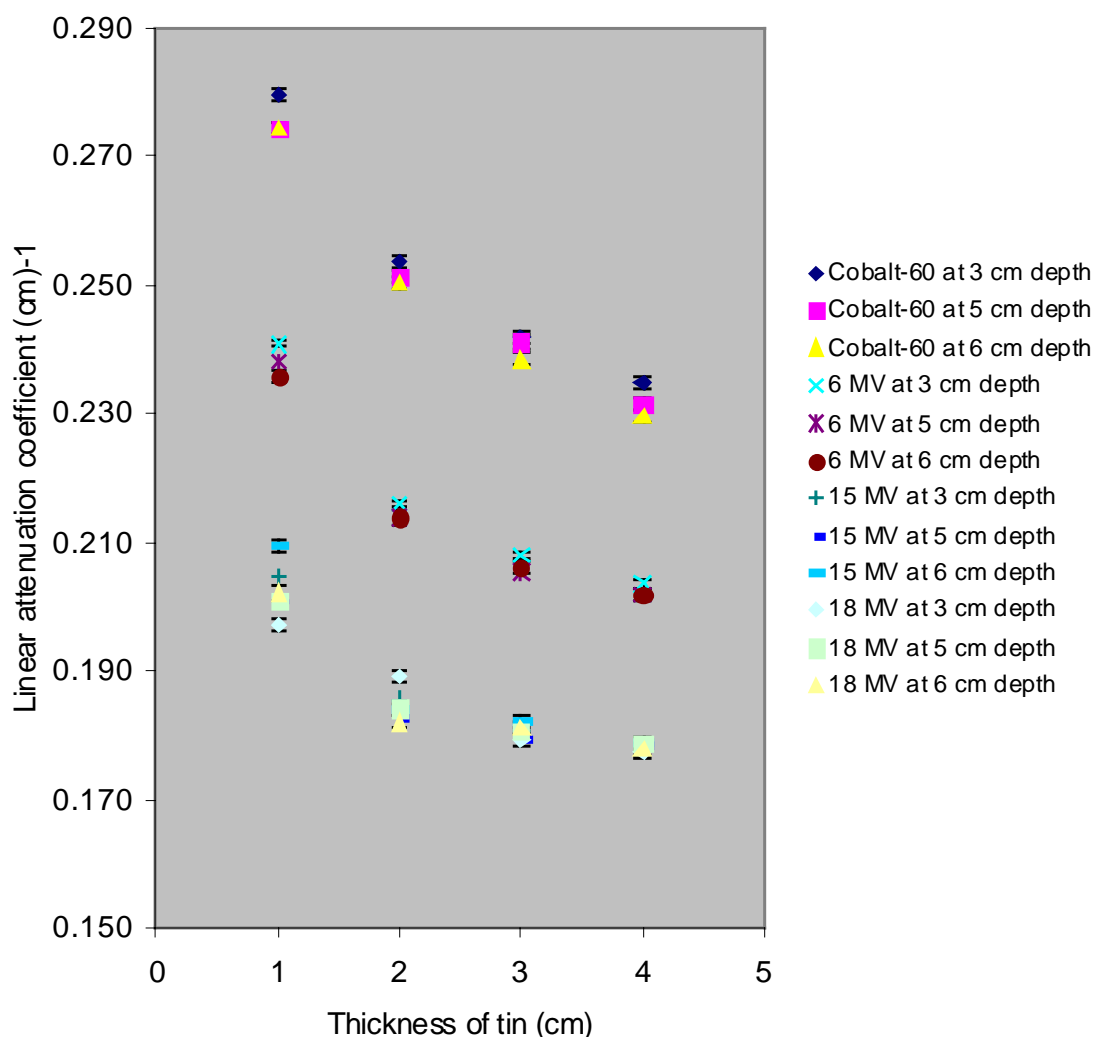


Figure 3- 1: Measured linear attenuation coefficients as a function of the thickness of the tin attenuator measured at different depths in a water phantom.

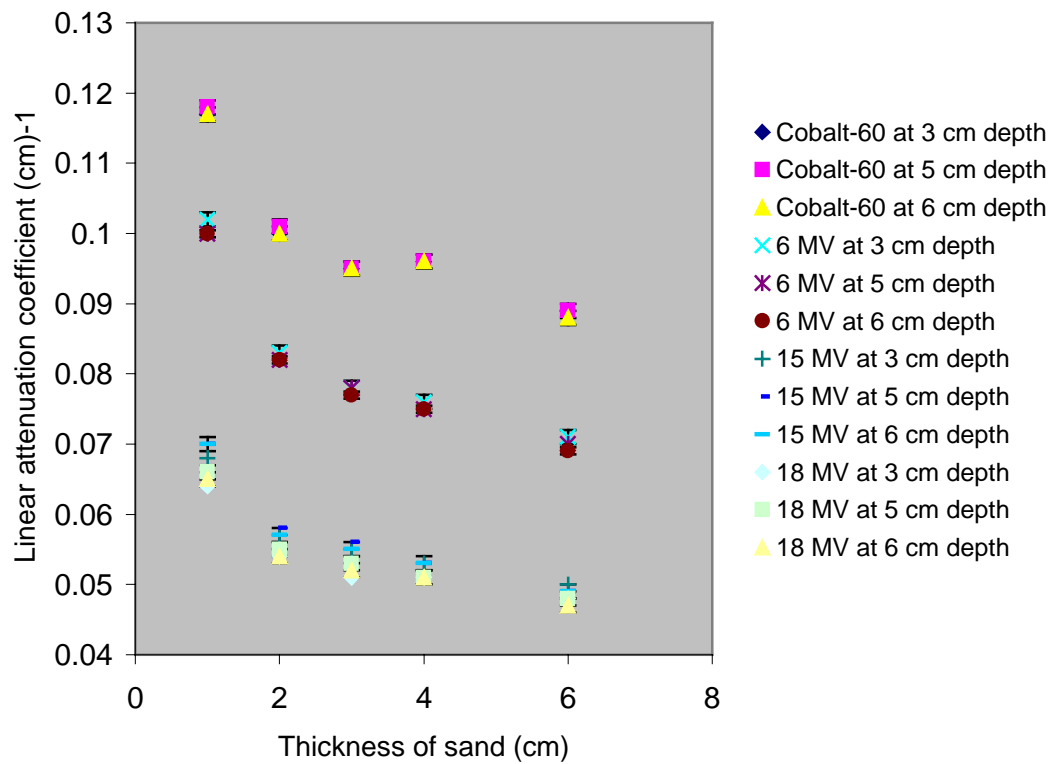


Figure 3- 2: Measured linear attenuation coefficients as a function of the thickness of the River sand mix attenuator measured at different depths in a water phantom.

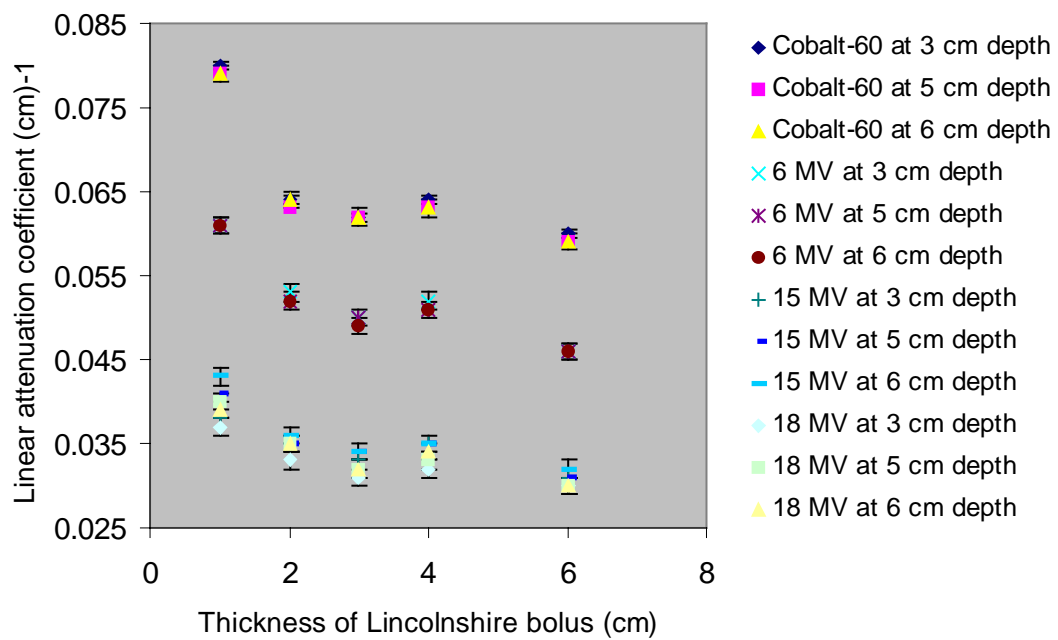


Figure 3- 3: Measured linear attenuation coefficients as a function of the thickness of the Lincolnshire bolus attenuator measured at different depths in a water phantom

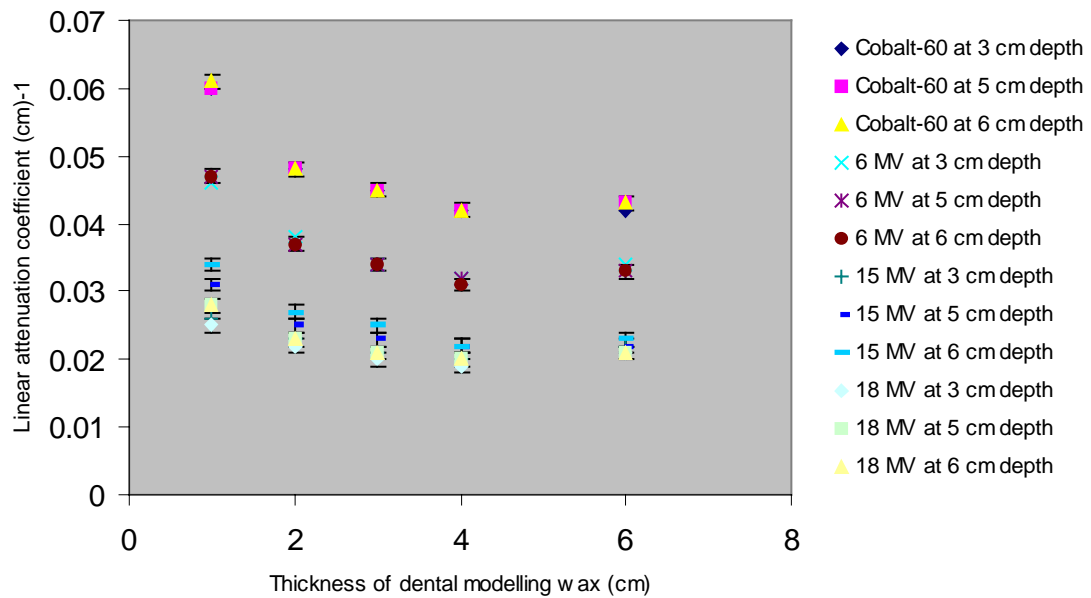


Figure 3- 4: Measured linear attenuation coefficients as a function of the thickness of the dental modelling wax attenuator measured at different depths in a water phantom.

For the same material and photon beam energy, the results did not indicate an appreciable change in the linear attenuation coefficients with depth for compensator thickness of more than 2 cm. Thus the depth of measurement in the phantom does not critically affect the linear attenuation coefficient of these materials in these photon beams.

The linear attenuation coefficients for each material type and thickness decreased with an increase in photon beam energy. The 15 MV and 18 MV data were almost the same for each material and at each measurement depth.

For each photon beam energy, the results indicated that the dental modelling wax had the lowest linear attenuation coefficient, followed by Lincolnshire bolus, River sand mix and then tin. Linear attenuation coefficients therefore increased with an increase in the density and atomic mass of the attenuator material.

For all materials and photon beam energies, the results indicated a smaller decrease in the linear attenuation coefficient with increase in attenuator thickness beyond 2 cm

thickness. Thus compensators calculated on average attenuation coefficients would not be very accurate for changes in surface contours of less than 2 cm.

Tissue maximum ratio (TMR) values measured in water on the machines indicated that the linear attenuation coefficients of the Lincolnshire bolus and dental modelling wax when corrected for density are very close to that of water. The linear attenuation coefficient values for Lincolnshire bolus are the closest to water in the ^{60}Co photon beam and increases relative to water with increasing photon beam energy. For dental modelling wax, the attenuation coefficient is closest to water at 18 MV photon beam energy and increases relative to water with decreasing photon beam energy. Selection of one of these compensator filling materials should therefore be based on the photon beam energy to be used.

3.2 Results of CT numbers and densities

The results of the CT numbers and the densities of the materials that were measured are shown in tables 3-1 and 3-2 respectively.

Table 3- 1: CT numbers of tin, River sand mix, high-density polystyrene, water, Lincolnshire bolus and dental modelling wax measured at three sequential CT mid slices S_1 , S_2 and S_3 .

Materials	CT numbers			
	S_1	S_2	S_3	Average
Tin	3280	3243	3368	3297 ± 64
River sand mix	612	684	593	630 ± 48
High-density polystyrene	124	125	128	126 ± 2
Water	7	2	5	5 ± 2
Lincolnshire bolus	- 70	- 75	-88	-78 ± 9
Modelling dental wax	-79	- 76	-109	-88 ± 18

Table 3- 2: Densities of tin, River sand mix, Lincolnshire bolus and dental modelling wax.

Material	Average density (g/cm^3)
Tin	7.3 ± 0.1
River sand mix	2.4 ± 0.0
Lincolnshire bolus	1.4 ± 0.0
Dental modelling wax	0.9 ± 0.0

These CT number results again indicated that Lincolnshire bolus and dental modelling wax were the closest to water. Their densities were also very close to water, which has a theoretical density of 1.00 g/cm^3 at STP. Thus Lincolnshire bolus and dental modelling wax can be used as near tissue equivalent materials in compensator design.

The CT numbers for River sand mix and tin of 630 ± 48 and 3297 ± 64 and their densities of $2.4 \pm 0.0 \text{ g/cm}^3$ and $7.3 \pm 0.1 \text{ g/cm}^3$ respectively, showed that these two materials are not very close to water. They would therefore require dilution with materials of low densities like low-density polystyrene if used in compensator construction. The CT number of the high-density polystyrene phantom used was 126 ± 2 . However, this is often considered to be tissue equivalent (AAPM TG-21, 1983)

Lincolnshire bolus was used as the compensating material in this work because the phantom studies were performed at 6 MV. Lincolnshire bolus is also quicker to prepare than dental modelling wax, which requires heating to shape and cooling to set. Lincolnshire bolus is also reusable although dental modelling wax has more uniformity in particle size.

3.3 Results for film dosimetry

Figures 3-5, 3-8 and 3-11 show the verification films for different treatment fields. Figures 3-6, 3-9 and 3-12 show the points around point O (0,0) taken as the origin of the treatment field of the verification films used for the film dosimetry. Similar points for each treatment field were selected at 1 cm and 2 cm equidistant from point O (0,0) and parallel to the major axes of the fields for breast and head and neck respectively.

To avoid optical density measurements in the region of penumbra, point O (0,0) was taken at the centre of the head and neck verification film with a treatment field of $14 \text{ cm} \times 15 \text{ cm}$. On the other hand, point O (0,0) was taken midline along the Y-axis and 4 cm measured from the posterior end of the field towards the anterior along the X-axis for both the verification films with treatment fields of $24 \text{ cm} \times 15 \text{ cm}$ for the right breast and $22 \text{ cm} \times 11 \text{ cm}$ for the left breast.

Figures 3-7, 3-10 and 3-13 show the correlation of the total dose deviation at each point relative to point O (0,0) for each treatment area using open fields, wedged fields and 3-D compensated treatment fields.

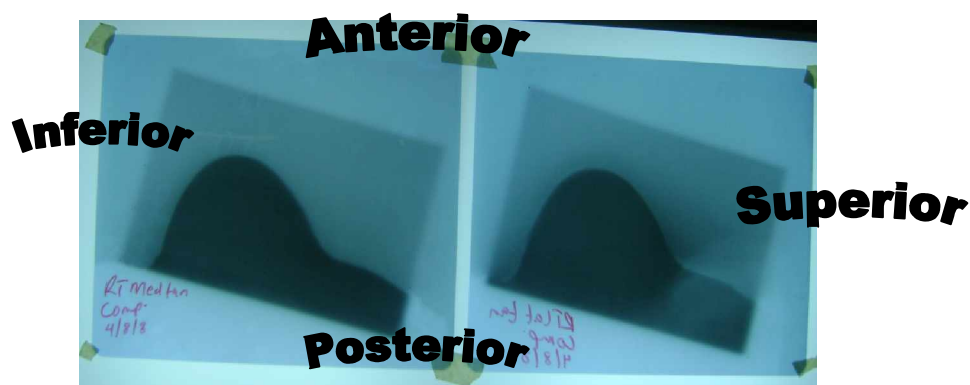


Figure 3- 5: Verification films of the 3-D compensated right breast medial and lateral tangential treatment fields (the same fields were used for the open and wedged fields).

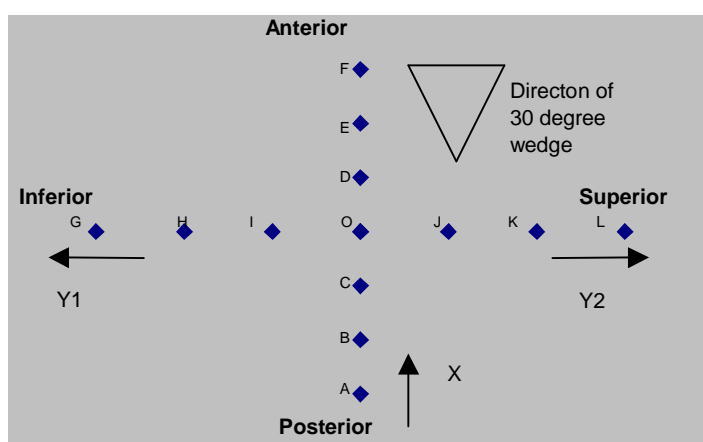


Figure 3- 6: The location of the points used on the six verification films relative to the point O (0,0) for the right breast (right medial and right lateral) tangential fields.

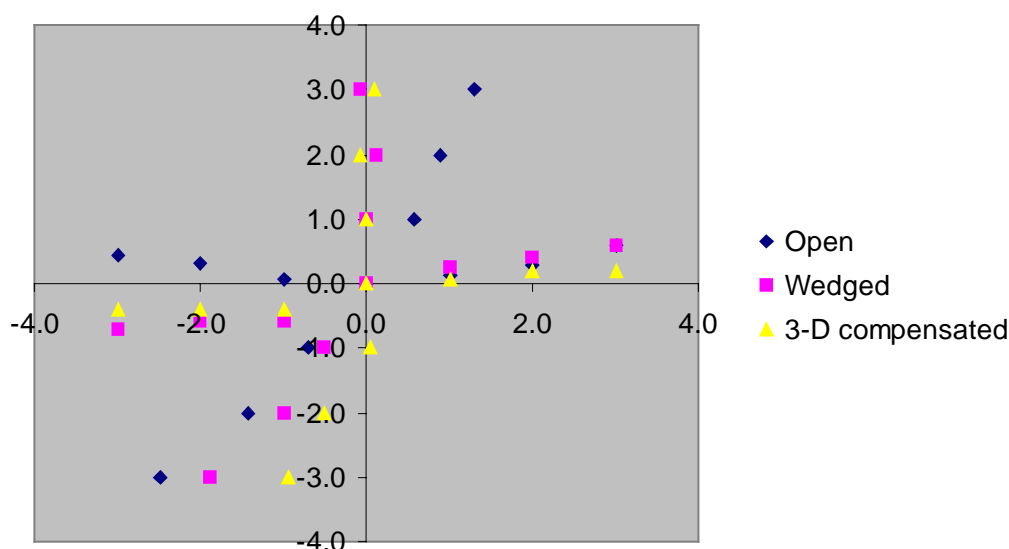


Figure 3- 7: The total dose deviation at each point relative to point O (0,0) for the right tangential breast treatment using open fields, wedged fields and 3-D compensated fields. An ideally compensated field would show alignment with the axes, i.e. no variation in dose throughout the field.

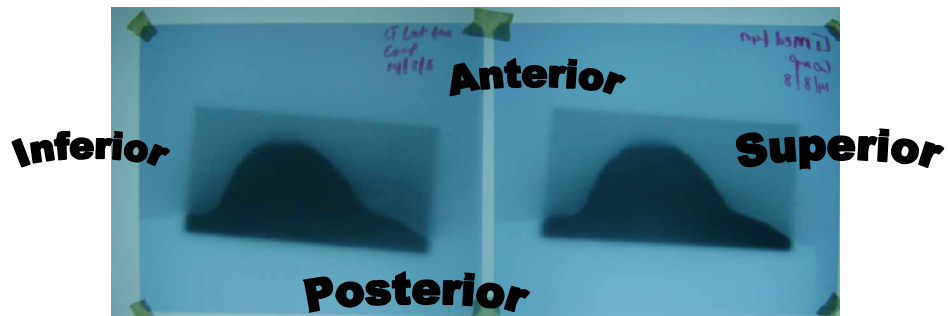


Figure 3- 8:Verification films of the 3-D compensated left breast medial and lateral tangential treatment fields (the same fields were used for the open and wedged fields).

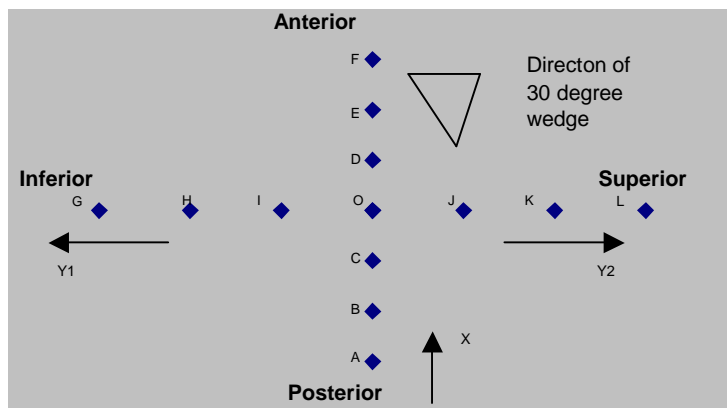


Figure 3- 9: The location of the points used on the six verification films relative to the point O (0,0) for the left breast (left medial and left lateral) tangential fields.

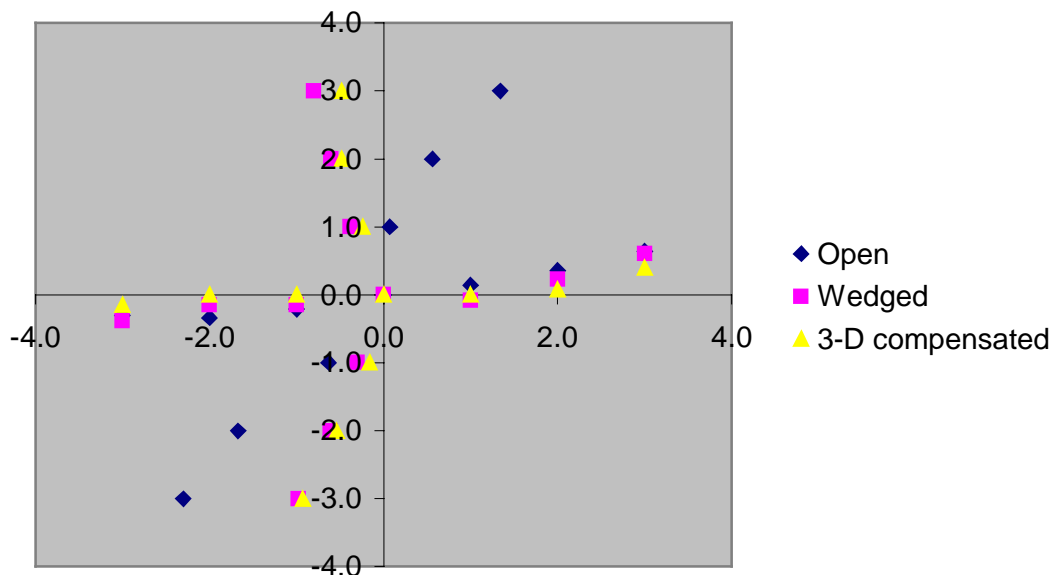


Figure 3- 10: The total dose deviation at each point relative to point O (0,0) for the left tangential breast treatment using open fields, wedged fields and 3-D compensated fields. An ideally compensated field would show alignment with the axes, i.e. no variation in dose throughout the field.



Figure 3- 11: Verification films of the 3-D compensated head and neck treatment fields (the same fields were used for the open and wedged fields).

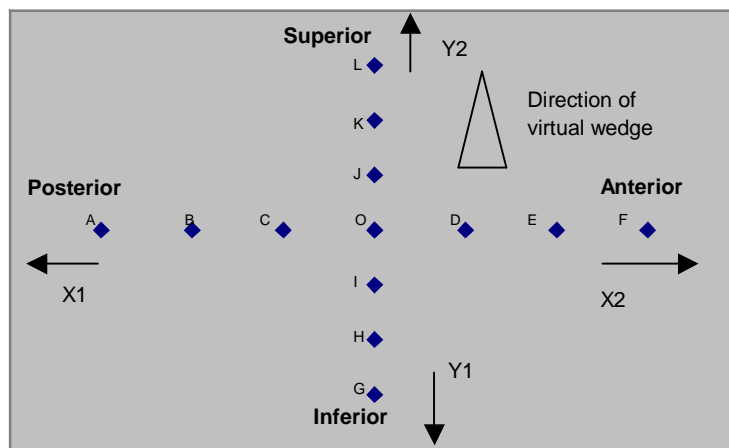


Figure 3- 12: The location of the points used on the six verification films relative to the point O (0,0) for the head and neck (right lateral and left lateral) treatment fields.

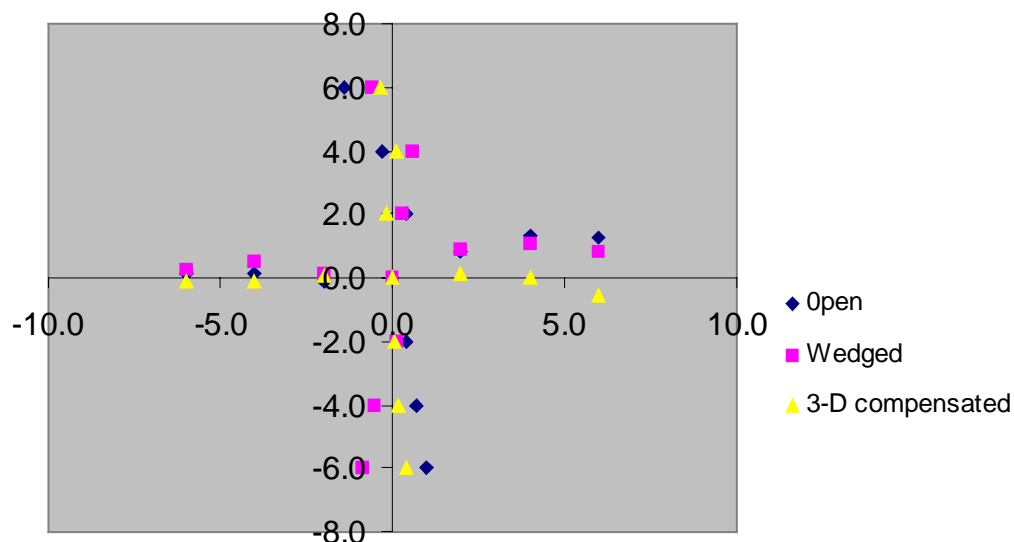


Figure 3- 13: The total dose deviation at each point relative to point O (0,0) for the head and neck treatment using open fields, wedged fields and 3-D compensated fields. An ideally compensated field would show alignment with the axes, i.e. no variation in dose throughout the field.

Results for the dose deviation at each point relative to point O (0,0) in figures 3-7, 3-10 and 3-13 indicate that for open fields, there was non-uniformity in the dose in all directions relative to the origin of the treatment field in the breast and head and neck cases. This confirms the non-uniformity in unmodified dose distribution.

The fields with wedges, showed an increased uniformity along the wedge direction. Non-uniformities were maintained in the non-wedged direction. This confirmed that the wedges could only compensate for dose non-uniformities resulting from wedge-shaped topographies. The overall dose uniformity improved compared to the open fields.

For the treatment fields with a 3-D missing tissue compensator, there was improved dose uniformity in all directions. The overall dose uniformity improved compared to the use of wedges. This confirms the effectiveness of the fabricated 3-D missing tissue compensators during treatment delivery.

More dose non-uniformity was measured in the posterior-anterior direction compared to the inferior-superior direction for the breast treatment fields. On the other hand, there was more dose non-uniformity in the inferior-superior direction compared to the posterior-anterior direction for the head and neck treatment fields. These reflect the greatest changes in surface topography over the treatment volumes in each case.

CHAPTER FOUR – RECOMMENDATION AND CONCLUSION

4.1 RECOMMENDATIONS

Lincolnshire bolus and dental modelling wax with measured CT numbers and densities close to water can be considered near tissue equivalent materials. They can be used as compensator filling materials without modification to the normal thickness of the missing tissue along a ray that requires a compensator of greater than 2 cm thickness. Tin and River sand mix cannot be used directly as tissue equivalent compensator filling materials with this methodology. Dilution with a low-density material for instance low-density polystyrene balls, castor sugar or rice, would be necessary similar to the production of the shelf materials like Lincolnshire bolus.

Broad-beam linear attenuation coefficients of materials were found to be dependent on photon beam energy, material density and thickness of the compensator but independent of the depth of measurement in the phantom for attenuators of thickness more than 2 cm.

The use of fabricated 3-D missing tissue compensators in megavoltage photon beams lead to a more uniform dose distribution of very irregular surface topographies such as breast and head and neck compared to open fields. Their use also resulted in better dose uniformity than that achieved by standard wedges only.

3-D missing tissue compensators can be fabricated cheaply using the 3-D manual missing tissue compensator cutter described in this report. This does not require a sophisticated 3-D treatment planning system. However,

- Correct breast and head and neck body surface contouring must be done at simulation to have good patient moulds.
- Negative moulds should be correctly mounted at the cutter using the correct jig system and following the appropriate quality control procedures presented in this report.
- The orthogonal laser system and the six movements of the cutter should be used correctly to align the mould correctly before cutting the Styrofoam.

- Complete positive moulds are not necessary to form casts; patient negative moulds can be correctly adjusted and aligned using the correct jig and orthogonal laser systems.
- If all the quality control procedures during the mounting of the breast mould at the cutter are followed, the manually fabricated 3-D missing tissue compensators correctly compensate for couch rotation during treatment delivery.

4.2 CONCLUSION

- 3-D missing tissue compensators give better uniformity in the dose distribution when used to treat very irregular surface topographies compared to unmodified fields or fields treated with wedges
- The compensators can be fabricated cheaply using the 3-D manual missing tissue compensator cutter described in this report. The correct quality control procedures documented in the report must be followed. This device provides a solution for many developing countries that cannot afford the expensive automated systems used with 3-D CT-based treatment planning systems.
- Lincolnshire bolus and dental modelling wax have attenuation properties close to water and are near tissue equivalent materials. Their use as compensator materials in this methodology does not require correction as would tin or River sand mix.

5 REFERENCES

- AAPM Task Group 21 (1983). A protocol for determination of absorbed dose for high-energy photon and electron beams. *Med. Phys*, vol. 10, pp. 746-771.
- Alderson, S.W., Lanzl, L.H., Rollins, M., Spira, J. (1962). An instrumentation phantom for analog computation of treatment plans. *The American Journal of Roentgenology, Radium Therapy and Nuclear Medicine*, vol. 87, pp. 185.
- Beck, G.G., McGonnagle, W.J., Sullivan, C.A. (1971). Use of a Styrofoam block cutter to make tissue-equivalent compensators. *Radiology*, vol. 100, pp. 694.
- Boge, R.J., Edland, R.W., Matthes, D.C. (1974). Tissue compensators for megavoltage radiotherapy fabricated from hollowed Styrofoam filled with wax. *Radiology*, vol. 111, pp. 193.
- Cosset, J.M. (March 2002). ESTRO Breur Gold Medal Award Lecture 2001, Irradiation accidents- lessons for oncology? *Radiotherapy and Oncology Journal of the European Society for Therapeutic Radiology and Oncology*.
- Dendy, P.P and Heaton, B. (1999). *Physics for Diagnostic Radiology*. 2nd ed. UK: IOP Publishing Ltd and individual contributors, pp. 59-62, and 88-89.
- Dimitriadis, D.M and Fallone, B.G. (2002). Compensators for intensity-modulated beams. *Medical Dosimetry*, vol. 27, no. 3, pp. 215-220.
- Dobbs, J., Barrett, A., Ash, D. (1999). *Practical Radiotherapy Planning*. 3rd ed. Great Britain: Arnold.
- Ellis, F., Hall, E.J., Oliver, R. (1959a). A compensator for variations in tissue thickness for high-energy beam. *Brit. J. Radiology*, vol. 32, pp. 421.
- Ellis, F and Lescrenier, C. (1973b). Combined compensation for contour and heterogeneity. *Radiology*, vol. 106, pp. 191.
- Feaster, G.R., Agarwal, S.K., Huddleston, A.L., Friesen, E.J. (1979). A missing tissue compensator. *Int. J. Radiation Oncology Biol. Phys*, vol. 5, pp. 277.
- Gunilla, C.B., Charles, E.N., Thomas, K.N. (1989). *Treatment Planning and Dose Calculation in Radiation Oncology*. 4th ed. USA: Pergamon press, pp. 45-46, 95-96, 203-205.
- Hall, E. J and Oliver, R. (1960). The use of standard isodose distributions with high-energy radiation beams-the accuracy of a compensator technique in correcting for body contours. *Brit. J. Radiology*, vol. 34, pp. 43.

IAEA Technical Report Series 115, (April 1994). *International Basic Safety Standards for Protection Against Ionising Radiation and for the Safety of Radiation Sources*. Vienna, Austria: IAEA, pp. 49-58.

Khan, F.M., Moore, V.C., Burns, D.J. (1968a). An apparatus for the construction of irregular surface compensators for use in radiotherapy. *Radiology*, vol. 90, pp. 593.

Khan, F.M., Moore, V.C., Burns, D.J. (1970b). The construction of compensators for cobalt teletherapy. *Radiology*, vol. 96, pp. 187-192.

Khan, F.M., Williamson, J.F., Sewchand, W., Kim, T.H. (1980c). Basic data for dosage calculation and compensation. *Int. J. Radiology Biol. Phys*, vol. 6, pp. 745.

Khan, F.M. (1994d). *The Physics of Radiation Therapy*. 2nd ed. 428 East Preston Street Baltimore, Maryland 21202 USA: Lippincott Williams and Wilkins, pp. 72-78, 263-264.

Khan, F.M. (2003e). *The Physics of Radiation Therapy*. 3rd ed. Philadelphia USA: Lippincott Williams and Wilkins, pp. 249-264.

Mira, J.G., Fullerton, G.D., Ezekiel, J., Potter, J.L. (1982). Evaluation of computed tomography numbers for treatment planning of cancer. *Int. J. Radiation Oncology Biol. Phys*, vol. 8, pp. 1625.

PACT. <http://www.iaea.org/pact/partnerships>

Papanikolaou, N., Battista, J.J., Boye, L.A., Kappas, C., Klein, E., Mackie, R.T., Sharpe, M., Van Dyk, J. (2004). *Tissue Inhomogeneity Corrections for Megavoltage Photon Beams*. 4513 Vernon Boulevard, Madison, WI 53705-4964: Medical physics publishing.

Podgorsak, E.B. (2005). *Radiation Oncology Physics: A handbook for teachers and students*. Austria: IAEA.

Purdy, J.A., Keys, D.J., Zivnuska, F. (1977). A compensator filter for chest portals. *Int. J. Radiation Oncology Biol. Phys*, vol. 2, pp. 1213.

Renner, W.D., O'Connor, T.P., Amtey, S.R., Reddi, P.R., Bahr, G.K., Kereiakes, J.G. (1977). The use of photogrammetry in tissue compensator designs part 1: Photogrammetric determination of patient topography. *Radiology*, vol. 125, pp. 505.

Shragge, P. C and Patterson, M. S. (1981). Improved method for the design of tissue compensators. *Medical Physics*, vol. 8, pp. 885.

Sundblom, L. (1964). Individually designed filters in cobalt-60 teletherapy. *Acta. Radiol. Ther. Phys Biol*, vol. 2, pp. 189.

- Stanton, R and Stinson, D. (1996). *Applied Physics for Radiation Oncology*. Madison Wisconsin: Medical physics publishing, pp. 98, 225-227, 232-235.
- Valentin, J. (November 2001). Recommendations for the prevention of accidental exposure in radiotherapy. *ELSEVIER Science Limited*.
- Van de Geijin, J. (1965). The construction of individualised intensity modifying filters in cobalt-60 teletherapy. *Brit. J. Radiology*, vol. 38, pp. 865.
- Van Dyk, J., Battista, J.J., Rider, W.D. (1980). Half body radiotherapy: The use of computed tomography to determine the dose to lung. *Int. J. Radiation Oncology Biol. Phys*, vol. 6, pp. 463.
- Weston, S. (June, 2008). Quality assurance of intensity modulated treatments. 48th Annual Congress of the South African Association of Physicists in Medicine and Biology (SAAPMB). Durban.

6 APPENDICES

APPENDIX A

Production and properties of photon beams

Photon beams are produced by x-ray generators like in linear accelerators or gamma rays emitted from a radioactive source like in ^{60}Co teletherapy units. These have no finite range and they are indirectly ionising type of radiation. They set secondary electrons in motion on passing through mater by the photoelectric or Compton effect. The secondary electrons produce ionisation of other atoms and molecules in the medium.

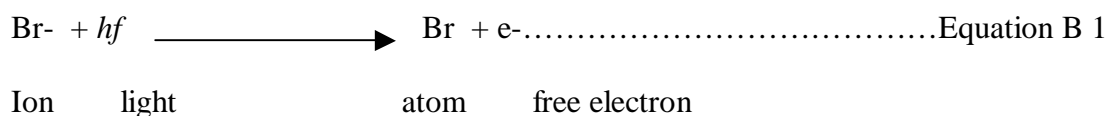
Whether it is a well-collimated monoenergetic or heteroenergetic photon beam passing through different thickness of materials, its beam intensity is reduced to some fraction of the initial value but never reduced to zero. The reduction in photon beam intensity is affected by thickness, density, and atomic number of the medium through which it is passing. However, the produced secondary electron have short finite ranges and their kinetic energy is rapidly dissipated first as ionisation and excitation, eventually as heat.

Effect of megavoltage photon radiation on the x-ray film

The x-ray film is composed of a base, an emulsion layer and a protective layer. The base is usually made of polyester. This maintains rigidity and carries the emulsion that is the sensitive part of the detector. The emulsion is protected from mechanical damage by the protective layer that is on both sides for double emulsion films or on one side for single emulsion films like those used in Mammography.

The emulsion is sensitive to both x-rays and light and thus should be kept in a light tight container. The film should only be loaded in a cassette using a special daylight loading system or in a dark room illuminated by a safe light. The emulsion of the film contains crystals of silver (Ag^+) and bromide (Br^-) ions that appear in cubic lattice. In a pure state they are electrically stable but the presence of impurities distort the crystal lattice producing a spot on the surface of the crystal called sensitivity speck.

On exposure to megavoltage beams, the Compton effect produces free electrons, which further displace electrons from the bromide ions according to equation B 1.



The free bromine atoms left behind are absorbed by gelatine that attaches the emulsion on to the base. The sensitivity speck traps the free electrons as they traverse the crystal. These trapped electrons attract the positively charged silver ion to the sensitivity speck that neutralises it to form silver atoms on the surface. This crystal is then the latent image. During development, the alkaline agent that is a reducing agent reduces the remaining silver ions in the areas with the crystal containing the latent image to form a dark silver grain speck on the film. The film is fixed and hardened using an acidic agent. The crystals that did not contain the latent image are washed off at fixation stage leaving a light area on the film (Dendy and Heaton, 1999). The optical density of the film is defined by equation B2.

$$D_o = \log_{10} (I_o/I) \dots \dots \dots \text{Equation B 2}$$

Where, I_o is the incident intensity reaching the film and I is the transmitted intensity through the film as shown in figure B1.

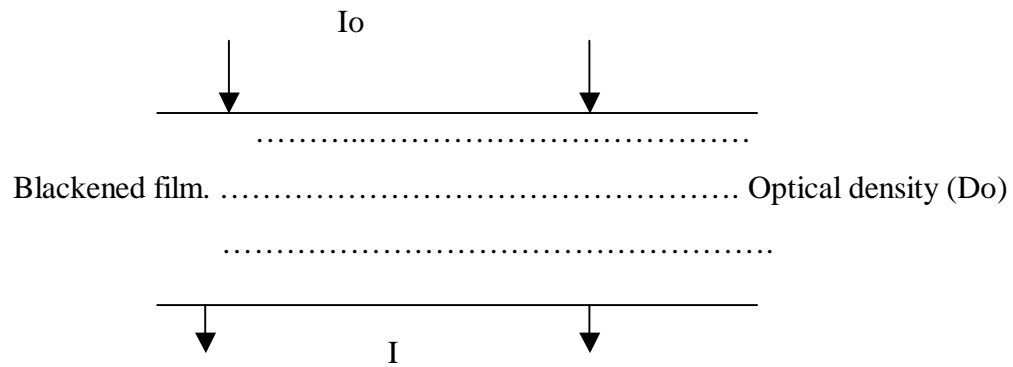


Figure B 1: Simple interpretation of optical density.

RANDO™ ALDERSON ANTHROMORPHIC PHANTOM

The RANDO™ Alderson anthropomorphic phantoms are moulded about natural male or female human skeletons in plastic materials that are radio-equivalent to soft tissues. They contain re-moulded lungs, radio-equivalent to human lung in a medium respiratory state. The air spaces of the head, neck and stem bronchi are duplicated as shown in figure C1. These are transacted at 2.5 cm intervals for insertion of dosimeters or film. Arms and legs are not included. Only the thorax portion and head and neck were used for this research report.

RANDO™ materials are matched to the human with respect to the effective atomic number, essential for low-energy equivalence and with respect to specific gravity, essential for high-energy equivalence. Thus radio-equivalence extends over the entire range from the lowest diagnostic to the highest therapeutic energies (Alderson *et al.*, 1962).

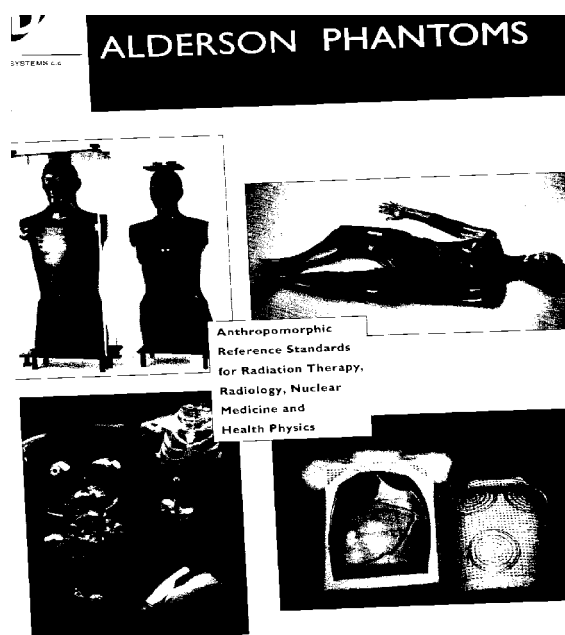


Figure C 1: Parts used to design The RANDO™ Alderson anthropomorphic phantoms.

The average-man RANDO™ Alderson anthropomorphic phantom corresponds to a body of 175 cm tall and mass of 73.5 kg whereas the average-woman RANDO™ Alderson anthropomorphic phantom corresponds to 163 cm tall and mass of 54 kg. Both the average man and woman RANDO™ Alderson anthropomorphic phantom present the same problems of treatment planning and administration, as do living patients of the same size, shape and skeletal structures. The only difference is that real patients permit detailed mapping of the dose distributions to enable treatment plans to be developed and tested realistically.